



**QUEEN'S
UNIVERSITY
BELFAST**

A statistical analysis of circumstellar material in Type Ia supernovae

Maguire, K., Sullivan, M., Patat, F., Gal-Yam, A., Hook, I. M., Dhawan, S., Howell, D. A., Mazzali, P., Nugent, P. E., Pan, Y. -C., Podsiadlowski, P., Simon, J. D., Sternberg, A., Valenti, S., Baltay, C., Bersier, D., Blagorodnova, N., Chen, T-W., Ellman, N., ... Young, D. R. (2013). A statistical analysis of circumstellar material in Type Ia supernovae. *Monthly Notices of the Royal Astronomical Society*, 436(1), 222-240.
<https://doi.org/10.1093/mnras/stt1586>

Published in:

Monthly Notices of the Royal Astronomical Society

Document Version:

Publisher's PDF, also known as Version of record

Queen's University Belfast - Research Portal:

[Link to publication record in Queen's University Belfast Research Portal](#)

Publisher rights

This article has been accepted for publication in Monthly Notices of the Royal Astronomical Society © 2013 The Authors Published by Oxford University Press on behalf of the Royal Astronomical Society. All rights reserved.

General rights

Copyright for the publications made accessible via the Queen's University Belfast Research Portal is retained by the author(s) and / or other copyright owners and it is a condition of accessing these publications that users recognise and abide by the legal requirements associated with these rights.

Take down policy

The Research Portal is Queen's institutional repository that provides access to Queen's research output. Every effort has been made to ensure that content in the Research Portal does not infringe any person's rights, or applicable UK laws. If you discover content in the Research Portal that you believe breaches copyright or violates any law, please contact openaccess@qub.ac.uk.

A statistical analysis of circumstellar material in Type Ia supernovae

K. Maguire,¹★ M. Sullivan,² F. Patat,³ A. Gal-Yam,⁴ I. M. Hook,^{1,5} S. Dhawan,¹
D. A. Howell,^{6,7} P. Mazzali,⁸ P. E. Nugent,^{9,10} Y.-C. Pan,¹ P. Podsiadlowski,¹
J. D. Simon,¹¹ A. Sternberg,¹² S. Valenti,^{6,7} C. Baltay,¹³ D. Bersier,⁸
N. Blagorodnova,¹⁴ T.-W. Chen,¹⁵ N. Ellman,¹³ U. Feindt,¹⁶ F. Förster,¹⁷ M. Fraser,¹⁵
S. González-Gaitán,¹⁷ M. L. Graham,^{6,7} C. Gutiérrez,¹⁷ S. Hachinger,¹⁸
E. Hadjiyska,¹³ C. Inserra,¹⁵ C. Knapic,¹⁹ R. R. Laher,²⁰ G. Leloudas,^{21,22}
S. Margheim,²³ R. McKinnon,¹³ M. Molinaro,¹⁹ N. Morrell,²⁴ E. O. Ofek,⁴
D. Rabinowitz,¹³ A. Rest,²⁵ D. Sand,²⁶ R. Smareglia,¹⁹ S. J. Smartt,¹⁵ F. Taddia,²⁷
E. S. Walker,¹³ N. A. Walton¹⁴ and D. R. Young¹⁵

¹Department of Physics (Astrophysics), University of Oxford, DWB, Keble Road, Oxford OX1 3RH, UK

²Physics & Astronomy, University of Southampton, Southampton, Hampshire SO17 1BJ, UK

³European Organisation for Astronomical Research in the Southern Hemisphere (ESO), Karl-Schwarzschild-Str. 2, D-85748 Garching b. München, Germany

⁴Ben-Zvi Center for Astrophysics, Weizmann Institute of Science, 76100 Rehovot, Israel

⁵INAF – Osservatorio Astronomico di Roma, via Frascati, 33, I-00040 Monte Porzio Catone, Roma, Italy

⁶Las Cumbres Observatory Global Telescope Network, Goleta, CA 93117, USA

⁷Department of Physics, University of California, Santa Barbara, CA 93106-9530, USA

⁸Liverpool John Moores, Liverpool Science Park, IC2 building, 146 Brownlow Hill, Liverpool L3 5RF, UK

⁹Cahill Center for Astrophysics, California Institute of Technology, East California Boulevard, Pasadena, CA 91125, USA

¹⁰Computational Cosmology Center, Lawrence Berkeley National Laboratory, 1 Cyclotron Road, Berkeley, CA 94720, USA

¹¹Observatories of the Carnegie Institution of Washington, 813 Santa Barbara St, Pasadena, CA 91101, USA

¹²Max-Planck-Institut für Astrophysik, Karl-Schwarzschildstr. 1, D-85748 Garching, Germany

¹³Department of Physics, Yale University, New Haven, CT 06250-8121, USA

¹⁴Institute of Astronomy, University of Cambridge, Madingley Road, Cambridge CB3 0HA, UK

¹⁵Astrophysics Research Centre, School of Mathematics and Physics, Queen's University Belfast, Belfast BT7 1NN, UK

¹⁶Physikalisches Institut, Universität Bonn, Nußallee 12, D-53115 Bonn, Germany

¹⁷Departamento de Astronomía, Universidad de Chile, Casilla 36-D, Santiago, Chile

¹⁸Julius-Maximilians-Universität Würzburg, Emil-Fischer-Str. 31, D-97074 Würzburg, Germany

¹⁹INAF – Osservatorio Astronomico di Trieste, Via G.B. Tiepolo 11, I-34143 Trieste, Italy

²⁰Spitzer Science Center, California Institute of Technology, M/S 314-6, Pasadena, CA 91125, USA

²¹The Oskar Klein Centre, Department of Physics, Stockholm University, AlbaNova, 10691 Stockholm, Sweden

²²Dark Cosmology Centre, Niels Bohr Institute, University of Copenhagen, Juliane Maries Vej 30, 2100 Copenhagen, Denmark

²³Gemini Observatory, Southern Operations Center, Casilla 603, La Serena, Chile

²⁴Las Campanas Observatory, Carnegie Observatories, Casilla 601, La Serena, Chile

²⁵Space Telescope Science Institute, 3700 San Martin Drive, Baltimore, MD 21218, USA

²⁶Texas Tech University, Physics Department, Box 41051, Lubbock, TX 79409-1051, USA

²⁷The Oskar Klein Centre, Department of Astronomy, Stockholm University, AlbaNova, 10691 Stockholm, Sweden

Accepted 2013 August 16. Received 2013 August 15; in original form 2013 July 12

ABSTRACT

A key tracer of the elusive progenitor systems of Type Ia supernovae (SNe Ia) is the detection of narrow blueshifted time-varying Na I D absorption lines, interpreted as evidence of circumstellar material surrounding the progenitor system. The origin of this material is controversial, but the simplest explanation is that it results from previous mass-loss in a system containing a white dwarf and a non-degenerate companion star. We present new single-epoch intermediate-resolution spectra of 17 low-redshift SNe Ia taken with XShooter on the

★E-mail: kate.maguire@astro.ox.ac.uk

European Southern Observatory Very Large Telescope. Combining this sample with events from the literature, we confirm an excess (~ 20 per cent) of SNe Ia displaying blueshifted narrow Na I D absorption features compared to redshifted Na I D features. The host galaxies of SNe Ia displaying blueshifted absorption profiles are skewed towards later-type galaxies, compared to SNe Ia that show no Na I D absorption and SNe Ia displaying blueshifted narrow Na I D absorption features have broader light curves. The strength of the Na I D absorption is stronger in SNe Ia displaying blueshifted Na I D absorption features than those without blueshifted features, and the strength of the blueshifted Na I D is correlated with the $B - V$ colour of the SN at maximum light. This strongly suggests the absorbing material is local to the SN. In the context of the progenitor systems of SNe Ia, we discuss the significance of these findings and other recent observational evidence on the nature of SN Ia progenitors. We present a summary that suggests that there are at least two distinct populations of normal, cosmologically useful SNe Ia.

Key words: circumstellar matter – supernovae: general – distance scale.

1 INTRODUCTION

Type Ia supernovae (SNe Ia) are excellent standardizable candles and play an important role in constraining cosmological parameters (e.g. Riess et al. 1998, 2007; Perlmutter et al. 1999; Kessler et al. 2009; Sullivan et al. 2011; Suzuki et al. 2012). However, there is still much debate over the nature of their progenitor systems. SNe Ia have long been suspected to be the result of the thermonuclear explosion of an accreting carbon–oxygen white dwarf (CO-WD) in a close binary system, and the compact nature of the exploding star has recently been confirmed observationally (Nugent et al. 2011; Bloom et al. 2012). However, the nature of the companion to the white dwarf (WD) remains unknown. Two main types of progenitor systems are generally considered: the double degenerate (DD; Iben & Tutukov 1984; Webbink 1984) scenario, with two WD, and the single degenerate (SD; Whelan & Iben 1973) scenario, with a non-degenerate companion star to the WD, such as a giant, sub-giant or main-sequence star. Recent observational evidence suggests that both of these channels may operate (Gilfanov & Bogdán 2010; Li et al. 2011; Sternberg et al. 2011; Dilday et al. 2012; Schaefer & Pagnotta 2012), although the relative frequency of each and the relation to host galaxy environment is not yet clear.

One observational tracer of different progenitor configurations is the detection of narrow time-varying blueshifted Na I D absorption features in SN Ia spectra (Patat et al. 2007; Blondin et al. 2009; Simon et al. 2009; Stritzinger et al. 2010). Such time-varying features, reminiscent of the spectra of both classical (Williams et al. 2008) and recurrent novae (Patat et al. 2011), are suggestive of outflowing material from the SN system, naturally explained by the SD scenario: non-accreted material from the donor star is blown away from the system prior to explosion and remains afterward as circumstellar material (CSM). The time-varying nature of the Na I D profiles suggests that the material is very close to the SN ($\sim 10^{16}$ – 10^{17} cm) and must be associated with the progenitor system. An interstellar origin for the variations caused by transverse proper motion in the absorbing material and/or line-of-sight effects can be ruled out since the Ca II H&K absorption features would also be expected to vary, which is not observed.

It was originally assumed that in the merger of two WD, CSM material would not be present. However, recent theoretical studies looking at both violent WD–WD mergers soon after the common envelope phase (Ruiter et al. 2013; Soker et al. 2013), as well as the interaction of ejected material from WD–WD binaries with the interstellar medium (ISM) have suggested that the DD channel may

be capable of producing CSM that could be detectable in some SNe Ia (Raskin & Kasen 2013; Shen, Guillochon & Foley 2013).

Sternberg et al. (2011) extended the single-object studies investigating time-varying Na I D absorption features, by searching for Na I D lines in single-epoch high-resolution spectra in a sample of 35 nearby SNe Ia. They showed that SNe Ia in spiral galaxies have a strong statistical preference for displaying blueshifted absorption structures in their spectra. Since only single-epoch spectra were obtained, the presence of blueshifted Na I D lines in any individual event does not directly imply the presence of CSM – some of these blueshifted (and all of the redshifted) features are expected to be due to the presence of interstellar absorption features. However, there is no reason to expect a preference for blueshifted over redshifted lines due to host galaxy material, and Sternberg et al. (2011) interpret their results as evidence for outflowing material in some SNe Ia in spiral galaxies. Using additional data from the literature combined with some new observations, Foley et al. (2012b) suggested that SNe Ia with blueshifted absorption profiles have, on average, higher Si II 6355 Å velocities and redder colours at maximum light relative to the rest of the SN Ia population. While the redder colours could be explained by an additional contribution of CSM to the SN colour (e.g. Amanullah & Goobar 2011), the Si II velocity trends are more difficult to explain.

In this paper, we present the results of an observational campaign to further link CSM signatures in SNe Ia with their photometric, spectral and host galaxy properties. We use intermediate-resolution spectra obtained over a multiperiod programme with the European Southern Observatory (ESO) Very Large Telescope (VLT) and the XShooter spectrograph to search for CSM signatures in a new sample of nearby SNe Ia. These data are complemented by light curves and spectra obtained through monitoring campaigns at multiple facilities to determine the relationship between SN Ia progenitor configurations and observed SN properties. Throughout this paper, we assume a Hubble constant of $H_0 = 70$ km s $^{-1}$ Mpc $^{-1}$.

2 OBSERVATIONS AND DATA REDUCTION

In this section, we present new observations of 17 SNe Ia that include intermediate-resolution spectra, complemented by low-resolution spectra and light-curve data. We combine our new data set with 16 events from the literature, giving a total sample of 33 events. We discuss the sample selection, spectroscopic observations and photometric monitoring in turn.

Table 1. Discovery details and host galaxy properties of the XShooter SN Ia sample.

SN name	RA (J2000)	Dec. (J2000)	Galaxy name	Heliocentric redshift (z_{heli})	Galaxy type ^a	Disc. source ^b	Disc. epoch	Spectroscopically classified ^c
LSQ12dbr	20:58:51.89	−02:58:27.1	Anon.	$0.0196 \pm 0.000\,344^e$	Irr ¹	LSQ	20120616	Gemini, ATel 4212
LSQ12fuk	04:58:15.89	−16:17:57.8	Anon.	$0.020\,20 \pm 0.000\,06^e$	Sab ¹	LSQ	20121031	NSF-II, ATel 4537
LSQ12fxd	05:22:16.99	−25:35:47.0	ESO 487–G 004	$0.031\,242 \pm 0.000\,017^f$	Sc	LSQ	20121101	PESSTO, ATel 4545
LSQ12gdj	23:54:43.32	−25:40:34.0	ESO 472–G 007	$0.030\,324 \pm 0.000\,057^f$	Sc	LSQ	20121107	NSF-II, ATel 4566
LSQ12hzj	09:59:12.43	−09:00:08.3	2MASX J09591230–0900095	0.029 ± 0.001^e	S0 ¹	LSQ	20121224	NSF-II, ATel 4701
PTF12iiq	02:50:07.76	−00:15:54.4	2MASX J02500784–0016014	$0.029\,08 \pm 0.000\,01^f$	S0 ¹	PTF	20120829	PTF, ATel 4363
PTF12jgb	04:15:01.44	−15:20:53.7	2MASX J0415016–152053	$0.028\,11 \pm 0.000\,08^e$	— ²	PTF	20121002	PTF, Gemini ⁱ
SN 2012cg ^d	12:27:12.83	+09:25:13.1	NGC 4424	$0.001\,538 \pm 0.000\,013^g$	Sa	LOSS	20120517	Lick, ATel 4115
SN 2012et ^d	23:42:38.82	+27 05 31.5	CGCG 476–117	$0.024\,78 \pm 0.000\,02^e$	Sb	TOCP	20120912	Asiago, CBET 3227
SN 2012fw ^d	21:01:58.99	−48:16:25.9	ESO 235–37	$0.018\,586 \pm 0.000\,150^f$	S0/a	TAROT	20120819	PESSTO, ATel 4339
SN 2012hd ^d	01:14:07.46	−32:39:07.7	IC 1657	$0.012\,18 \pm 0.000\,02^e$	Sbc	TOCP	20121121	PESSTO, ATel 4602
SN 2012hr ^d	06:21:38.46	−59:42:50.6	ESO 121–26	$0.007\,562 \pm 0.000\,013^f$	Sbc	TOCP	20121217	CSP, ATel 4663
SN 2012ht ^d	10:53:22.75	+16:46:34.9	NGC 3447	$0.003\,559 \pm 0.000\,04^f$	Irr ¹	TOCP	20121219	Asiago, CBET 3350
SN 2013U ^d	10:01:12.00	+00:19:42.3	CGCG 8–23	$0.034\,17 \pm 0.000\,08^e$	Sc	TOCP	20130205	Asiago, ATel 4796
SN 2013aa ^d	14:32:33.88	−44:13:27.8	NGC 5643	$0.003\,999 \pm 0.000\,007^f$	Sc	TOCP	20130214	FLOYDS, ATel 4817
SN 2013aj ^d	13:54:00.68	−07:55:43.8	NGC 5339	$0.009\,126 \pm 0.000\,010^f$	Sa pec	TOCP	20130303	PESSTO, ATel 4852
SN 2013ao ^d	11:44:44.74	−20:31:41.1	Anon.	$\sim 0.04^h$	Dwarf ¹	CRTS	20130304	PESSTO, ATel 4863

^aSource of galaxy classification is NED unless otherwise noted. ¹Visually classified for this paper. ²Classification of the host of PTF12jgb is unclear from available images.

^bDiscovery source description is given in Section 2.1

^cThe telescope or collaboration that spectroscopically classified the SN. Further details can be found in the listed ATel or CBET.

^dAlternative names and additional references: SN 2012cg (Silverman et al. 2012c), SN 2012et = PSN J23423882+2705315 (CBET 3227), SN 2012fw = PSN J21015899–4816259 (CBET 3282), SN 2012hd = LSQ12gqn (CBET 3324), SN 2012hr = PSN J06213846–5942506 (CBET 3346), SN 2012ht = PSN J10532275+1646349, SN 2013U = PSN J10011200+0019423 (CBET 3410), SN 2013aa = PSN J14323388–4413278 (CBET 3416), SN 2013aj = PSN J13540068–0755438 (CBET 3434), SN 2013ao = SSS 130304:114445–203141 (ATel 4908, CBET 3442).

^eRedshift measured from host galaxy features in SN spectrum. ^fRedshift from recessional velocity obtained from NED or SDSS Data Release 9.

^gRedshift calculated from the stellar velocity field of Cortés, Kenney & Hardy (2006) at the position of SN 2012cg.

^hA redshift for SN 2013ao is not listed in NED/SDSS and no host galaxy lines are identified in any of its spectra. A redshift of ~ 0.04 is obtained from SN spectral fitting but does not have the necessary accuracy for this study.

ⁱNo ATel or CBET was released for PTF12jgb. It was classified at Gemini North using the Gemini Multi-Object Spectrograph (GMOS) by the PTF collaboration on 20121004 as an SN Ia.

2.1 Sample selection

The new SN Ia data were obtained over the course of a multiperiod programme at the VLT using the XShooter spectrograph (Vernet et al. 2011). Details of the 17 SNe Ia, discovered by a variety of surveys/searches, are listed in Table 1. The SNe were selected according to the following two criteria: (i) the SNe were located at $z < 0.03$ to enable a high signal-to-noise spectrum to be obtained and (ii) the SNe were spectroscopically classified as SNe Ia prior to maximum light, so that a reliable light curve could be measured. We did not preferentially select SNe Ia displaying redder optical colours or strong Na I D absorption features in the low-resolution classification spectra (as was historically the case) to ensure an unbiased sample. Not all SNe Ia discovered during the programmes that fulfilled these criteria were observed due to scheduling constraints at VLT UT2.

The primary source of our targets was amateur searches, with discoveries taken from the Transient Objects Confirmation Page (TOCP¹). Additional events were discovered by the Palomar Transient Factory (PTF; Law et al. 2009; Rau et al. 2009), La Silla Quest Variability Survey (LSQ; Baltay et al. 2012), the Catalina Real-Time Transient Survey (CRTS; Drake et al. 2009), the Lick Observatory Supernova Search (LOSS; Leaman et al. 2011) and the Télescope à Action Rapide pour les Objets Transitoires (TAROT; Klotz et al. 2008).

Some of the SNe were classified as part of the ESO Large Programme, Public ESO Spectroscopic Survey of Transient Objects² (PESSTO), which is currently operating at the New Technology Telescope, La Silla, Chile. Additional observations of SN 2012cg are detailed in Silverman et al. (2012c) and Munari et al. (2013). Nearly all of the SNe Ia in the sample are spectroscopically similar to ‘normal’ SNe Ia, with the exception of SN 2013ao (spectroscopically similar to a ‘super-Chandrasekhar’ SN Ia; Howell et al. 2006), SN 2013U (classified as a 1991T-like object) and LSQ12gdj, a second ‘super-Chandrasekhar’ SN Ia (Scalzo et al., in preparation). SN 2013ao is excluded from further discussion because a spectroscopic redshift for its host galaxy could not be determined, and hence the velocity measurements are less reliable.

2.2 Spectroscopy

Intermediate-resolution spectra were obtained for all SNe using XShooter under target-of-opportunity programmes, IDs 089.D-0647(A) and 090.D-0828(A). XShooter is an echelle spectrograph with three arms (UV, visible and near-infrared) covering the wavelength range of 3000–25 000 Å. The instrumental resolution of the spectrograph is fixed, and we used the narrowest available slit

¹ <http://www.cbat.eps.harvard.edu/unconf/tocp.html>

² <http://www.pessto.org/pessto/index.py>

Table 2. Intermediate resolution XShooter spectral information and derived light-curve properties. The sample is split based on the presence of ‘blueshifted’, ‘non-blueshifted’ or no narrow absorption features of Na I D in their spectra, as discussed in Section 3.1.

SN name	Date of spec.	MJD ^a of spec.	Phase ^b (d)	MJD of <i>B</i> -band max.	Stretch	<i>B</i> – <i>V</i> at max.	LC source ^c	Na I D ₂ pEW (Å)	‘Blueshifted’ Na I D ₂ pEW (Å) ^d
Blueshifted Na I D									
LSQ12fxd	20121113	562 44.2	–1.9	562 46.1 ± 0.1	1.121 ± 0.016	–	LSQ	0.50 ± 0.01	0.50 ± 0.01
LSQ12gdj	20121118	562 49.0	–4.4	562 53.4 ± 0.1	1.130 ± 0.008	0.00 ± 0.01	Scalzo et al.	0.05 ± 0.03	0.05 ± 0.03
SN 2012cg*	20120603	560 81.0	–0.8	560 81.8 ± 0.4	1.098 ± 0.022	0.14 ± 0.04	LT+RATCam ^e	0.96 ± 0.02	0.62 ± 0.05
	20120630	561 09.0	+27.3	560 81.8 ± 0.4	1.098 ± 0.022	0.14 ± 0.04	LT+RATCam ^e	0.96 ± 0.02	0.62 ± 0.05
SN 2012et	20120930	562 01.1	+11.1	561 90.0 ± 1.1	1.194 ± 0.098	0.16 ± 0.03	LT+IO:O, P48	0.65 ± 0.04	0.65 ± 0.04
SN 2012hd*	20121127	562 58.1	–6.7	562 64.8 ± 0.8	0.957 ± 0.095	–	FTS, LSQ	1.02 ± 0.03	0.54 ± 0.03
SN 2013U	20130212	563 36.2	–1.6	563 37.8 ± 0.3	1.091 ± 0.070	–	LT+IO	0.88 ± 0.02	0.68 ± 0.03
SN 2013aj	20130310	563 60.3	+0.8	563 59.5 ± 0.6	0.911 ± 0.054	0.02 ± 0.02	LT+IO:O, SMARTS	0.21 ± 0.01	0.21 ± 0.01
Non-blueshifted Na I D									
LSQ12fuk*	20121106	562 37.2	+4.6	562 32.6 ± 0.2	0.999 ± 0.051	–	P48	0.24 ± 0.02	–
SN 2012hr	20121222	562 83.1	–6.1	562 89.2 ± 0.1	1.018 ± 0.021	0.03 ± 0.01	LCOGT 1m	0.12 ± 0.01	–
SN 2012fw	20120904	561 74.1	+7.2	561 66.9 ± 0.7	1.135 ± 0.073	0.11 ± 0.02	FTS	0.24 ± 0.01	–
No Na I D									
LSQ12dbr	20120702	561 10.4	–0.3	561 10.7 ± 0.2	1.085 ± 0.014	–0.13 ± 0.02	LSQ, LT+RATCam	–	–
LSQ12hzj	20130109	563 01.3	+0.7	563 00.6 ± 0.2	0.931 ± 0.035	–	LSQ	–	–
PTF12iiq	20120908	561 78.3	–3.8	561 82.1 ± 0.3	0.925 ± 0.028	0.10 ± 0.02	LT+RATCam, P48	–	–
PTF12jgb	20121009	562 09.3	+5.4	562 03.9 ± 0.6	1.230 ± 0.073	–	LT+IO:O, P48	–	–
SN 2012ht	20121231	562 93.3	–1.6	562 94.9 ± 0.2	0.877 ± 0.022	–0.04 ± 0.02	LT+IO:O	–	–
SN 2013aa	20130223	563 47.3	+3.3	563 44.0 ± 0.1	1.146 ± 0.019	–0.05 ± 0.01	LCOGT 1m	–	–

^aModified Julian date.^bPhase with respect to *B*-band maximum.^cFurther information on the telescopes and instruments used can be found in Section 2.3.^d‘Blueshifted’ Na I D pEW refers to the integrated pEW of any Na I D₂ absorption features that are blueshifted with respect to the defined zero-velocity position.^eLT light-curve data were supplemented using data from Munari et al. (2013).

*SN 2012hd and LSQ12fuk are removed from our calculation of the ratio of ‘blueshifted’ to ‘redshifted’ absorption features in Section 3.3 for the following reasons: SN 2012hd and SN 2012cg because they display both ‘blueshifted’ and ‘non-blueshifted’ Na I D absorption components and LSQ12fuk because its absorption is a single component at zero velocity.

widths of 0.5 arcsec (UV arm), 0.4 arcsec (visible arm) and 0.4 arcsec (near-infrared arm) to achieve resolutions of $R \sim 9900$, 18 200 and 10 500, respectively. These resolutions are necessary to resolve the narrow Na I D (5890, 5896 Å), Ca II H&K (3934, 3969 Å) and K I (7665, 7699 Å) features of interest for this study. Due to the narrow slits employed and lack of atmospheric dispersion correctors for XShooter at the time of observations, the absolute flux calibration is uncertain. However, we are interested in the shifts in wavelength position and the relative strengths of features so this does not affect our results. Details of the XShooter spectral observations are listed in Table 2. The spectra were reduced using the public XShooter pipeline, which performs a full reduction of the spectral orders in each of the three arms to obtain a contiguous one-dimensional merged spectrum (Modigliani et al. 2010). Spectra showing the Na I D and Ca II H&K narrow absorption features are displayed in Figs 1–3 for the whole sample. XShooter spectra of SN 2012cg were obtained on two occasions, with both shown in Fig. 1. The selection of velocity zero-points for the sample is discussed in Section 3.

Follow-up low-resolution optical spectra were obtained for our SN sample and details are given in Table 3. These low-resolution spectra were reduced using custom pipelines for each of the telescopes based on standard spectral reduction procedures in IRAF and IDL. The two-dimensional spectra were bias and flat-field corrected before extraction. The extracted spectra were calibrated in wavelength using arc-lamp exposures and instrumental response functions were obtained from observations of spectrophotometric standards to perform the flux calibration.

2.3 Optical photometry

The optical photometry of the SNe Ia comes from six facilities: (i) the PTF search telescope, the Palomar 48 in (P48), (ii) the LSQ search telescope, the 40 arcsec ESO Schmidt Telescope, (iii) the robotic 2 m Liverpool Telescope (LT; Steele et al. 2004), (iv) the Faulkes Telescope South (FTS), (v) Las Cumbres Observatory Global Telescope (LCOGT) 1 m telescope array in Chile, part of the LCOGT network (Brown et al. 2013) and (vi) the Small & Moderate Aperture Research Telescope System (SMARTS) 1.3 m telescope at Cerro Tololo Inter-American Observatory (CTIO), Chile. *g'*- and *R*-band data were taken with the P48, and reduced using the Infrared Processing and Analysis Center (IPAC)³ pipeline (Laher et al., in preparation) and photometrically calibrated (Ofek et al. 2012). The LSQ telescope observes in a wide ‘*g+r*’ filter, while the LT data were obtained using both the RATCam and Infrared-Optical:Optical (IO:O) optical imagers in *gri* filters, similar to those used in the Sloan Digital Sky Survey (SDSS; York et al. 2000). Data from FTS, a clone of the LT, were obtained with the SPECTRAL imager in *gri* filters, while data from the LCOGT 1 m array were obtained in Johnson–Cousins *UBVRI* and SDSS-like *gri* filters. SMARTS data were obtained using the optical–infrared imager, ANDICAM in KPNO *BVRI* filters. Photometric data of superluminous SN Ia, LSQ12gdj will be presented in Scalzo et al. (in preparation) and is used here to calculate a light-curve width and colour.

³ <http://www.ipac.caltech.edu/>

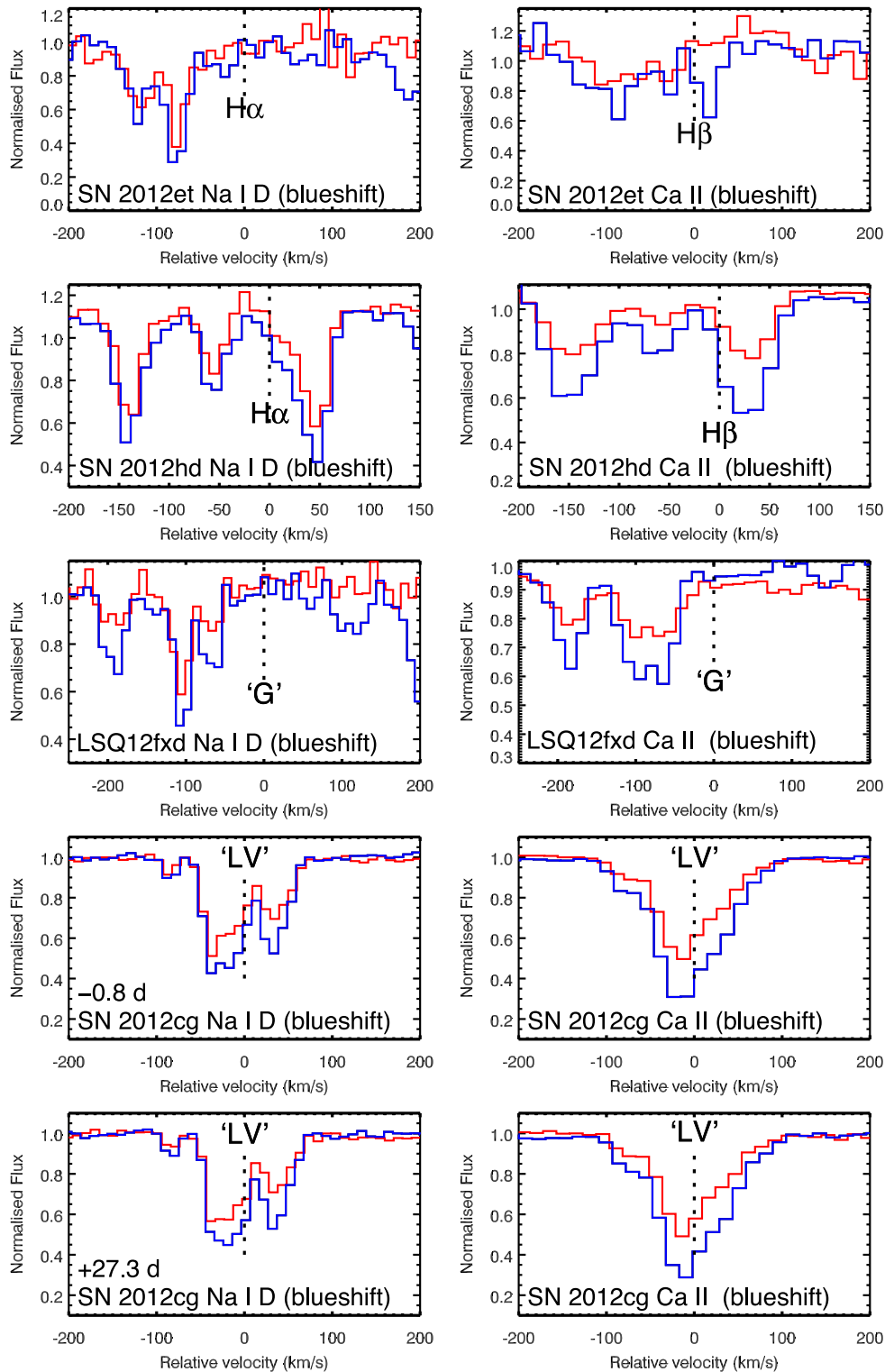


Figure 1. Intermediate-resolution VLT+XShooter spectra of the Na I D absorption lines in the left-hand panels (Na I D₁ is in red, Na I D₂ is in blue) and the Ca II H&K lines on the right (Ca II H is red, Ca II K is in blue). The velocity scale is plotted with a zero velocity defined by the position of the host galaxy features, marked with ‘H α ’ and ‘H β ’. If galaxy lines are not visible, the rest wavelength is defined by the recessional velocity of the host galaxy obtained from NED, and is marked with a ‘G’ on the spectra. For SN 2012cg, the local velocity (‘LV’) at the SN position was measured from the stellar velocity maps of Cortés et al. (2006). Two spectra of SN 2012cg were obtained at -0.8 d and $+27.3$ d with respect to B -band maximum. All SNe Ia in this figure display at least one absorption component that is blueshifted (‘blueshift’).

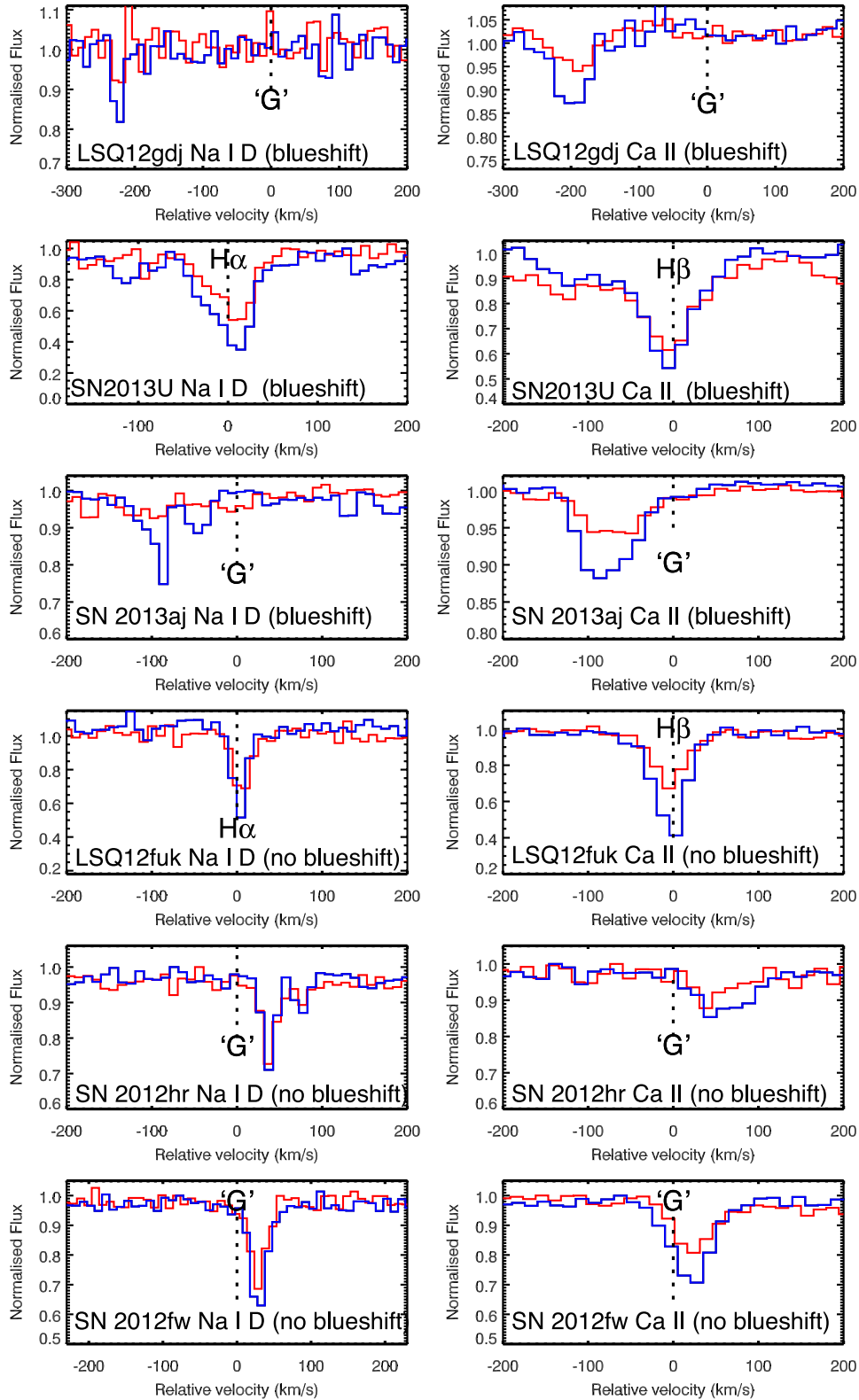


Figure 2. As Fig. 1. SNe Ia displaying ‘blueshifted’ absorption features are marked as ‘blueshift’, while those not displaying any blueshifted features are labelled as ‘no blueshift’.

The SN magnitude was measured on each epoch using Point Spread Function (PSF) photometry and calibrated using tertiary standard stars in the field of the SN. Where available, the zero-points of the images were calculated using aperture photometry

by comparing tertiary stars in the field directly with their SDSS magnitudes. If this was not possible, stars in the SN fields were calibrated using standard star observations on photometric nights and used to estimate a nightly zero-point. Uncertainties on the SN

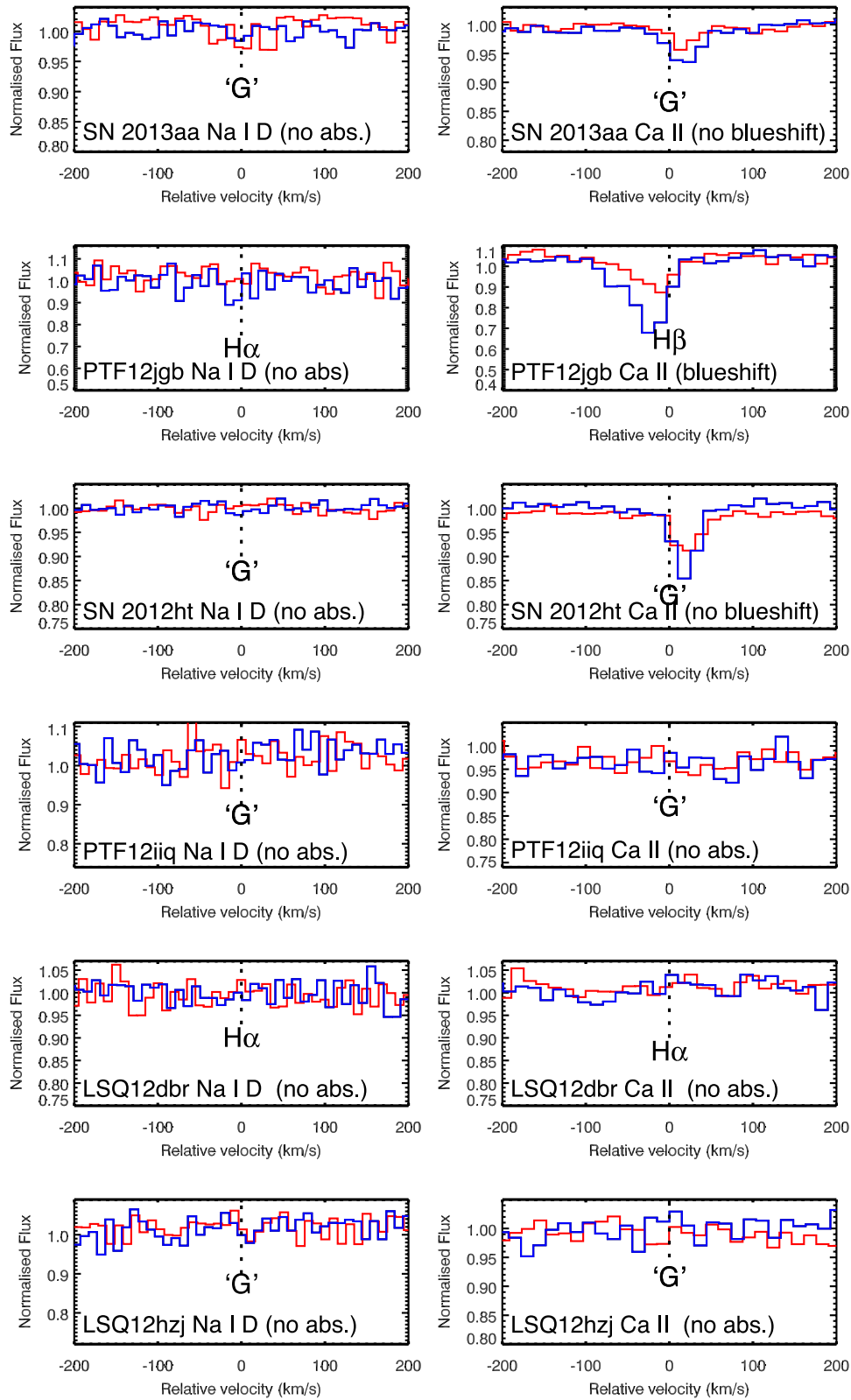


Figure 3. As Fig. 1. None of the SNe Ia in this figure display absorption features at the wavelength of Na I D and are labelled as ‘no abs.’ At the wavelength of Ca II H&K, one SN Ia shows blueshifted, two show non-blueshifted and three show no Ca II H&K absorption.

Table 3. Low-resolution spectral information for follow-up spectra of our XShooter sample used for measuring the Si II 6355 Å velocities. The order of the SNe is following that of Table 2.

SN name	Date	MJD	Phase (d)	Telescope+instrument ^a	Wavelength range (Å)	Si II 6355 Å vel. 10 ³ km s ⁻¹
LSQ12fxd	20121112	562 44.2	-1.9	VLT + XSH	3100–24 790	10.97 ± 0.10
LSQ12fxd	20121112	562 44.3	-1.8	NTT + EFOSC2	3368–10 300	10.94 ± 0.14
LSQ12gdj	20121122	562 54.2	+0.8	NTT + EFOSC2	3368–10 300	10.83 ± 0.10
SN 2012cg	20120603	560 81.0	-0.8	VLT + XSH	3100–24 790	10.42 ± 0.10
SN 2012hd	20121206	562 68.2	+3.4	NTT + EFOSC2	3368–10 300	9.73 ± 0.10
SN 2013U	20130212	563 36.2	-1.6	VLT + XSH	3100–24 790	9.94 ± 0.13
SN 2013aj	20130310	563 60.3	+0.8	VLT + XSH	3100–24 790	10.98 ± 0.10
LSQ12fuk	20121106	562 37.2	+4.6	VLT + XSH	3100–24 790	9.89 ± 0.18
SN 2012hr	20121223	562 84.6	-4.6	FTS + FLOYDS	3150–10 950	12.61 ± 0.13
SN 2012hr	20130101	562 94.3	+5.3	NTT + EFOSC2	3368–10 300	11.05 ± 0.12
SN 2012fw	20120826	561 66.1	-0.8	NTT + EFOSC2	3985–9315	9.76 ± 0.11
LSQ12dbr	20120702	561 10.4	-0.3	VLT + XSH	3100–24 790	11.41 ± 0.11
LSQ12hzj	20130109	563 01.3	+0.7	VLT + XSH	3100–24 790	9.02 ± 0.31
PTF12jgb	20121004	562 05	0	Gemini-N + GMOS	3400–9450	9.99 ± 0.10
SN 2012ht	20120231	562 93.3	-1.6	VLT + XSH	3100–24 790	10.99 ± 0.11
SN 2012ht	20130101	562 94.3	-0.6	NTT + EFOSC2	3368–10 300	11.02 ± 0.10
SN 2013aa	20130219	563 42.7	-1.3	FTS + FLOYDS	3150–10 950	10.71 ± 0.16
SN 2013aa	20130223	563 47.3	+3.3	VLT + XSH	3100–24 790	10.21 ± 0.10
SN 2013aa	20130225	563 48.4	+4.4	Gemini-S + GMOS	4200–8400	10.19 ± 0.14

^aInformation on the telescopes and instruments used:

VLT+XSH = VLT at Paranal, Chile, with the XShooter spectrograph.

NTT+EFOSC2 = New Technology Telescope, La Silla, Chile, with the ESO Faint Object Spectrograph and Camera 2.

FTS+FLOYDS = Faulkes Telescope South, Siding Spring, Australia, with the FLOYDS spectrograph.

Gemini-N+GMOS = Gemini Telescope North, Mauna Kea, Hawaii, US, with the Gemini Multi-Object Spectrograph.

Gemini-S+GMOS = Gemini Telescope South, Cerro Pachon, Chile, with the Gemini Multi-Object Spectrograph.

flux measurements are a combination of the statistical and calibration uncertainties and are inputted to the light-curve fitting routine, detailed in Section 2.4.

2.4 Light-curve fitting

The optical light curves were analysed using the SiFTO light curve fitting code (Conley et al. 2008), which produces values for the stretch (s ; light-curve width), maximum B -band magnitude, $B - V$ at maximum (where multiple bands are available) and time of maximum light for each SN. These values for our sample are given in Table 2. SiFTO uses a time series of spectral templates that are adjusted to recreate the observed colours of the SN photometry at each epoch, while also adjusting for Galactic extinction and redshift (i.e. the k -correction). The unknown contribution of the host galaxy to extinction has not been corrected for. All of the SNe Ia in our sample fall within the light-curve width range used in cosmological studies ($0.7 < s < 1.3$).

2.5 SN photospheric Si II velocity measurements

SNe Ia with ‘blueshifted’ Na I D absorption features (with respect to the strongest Na I D component) have been suggested to have higher Si II 6355 Å velocities near maximum light relative to the SN Ia population as a whole (Foley et al. 2012b). Therefore, we measure the velocities of Si II 6355 Å feature in near-maximum light spectra for our sample.

The Si II 6355 Å velocities were measured using a Gaussian fit to the feature, broadly following the method described in Maguire et al. (2012). Briefly, the pseudo-continuum is defined using a region on each side of the feature and then the observed spectrum is divided by this continuum. The position of the minimum of the feature

is measured by fitting a Gaussian to the feature using the MPFIT (Markwardt 2009) procedure in IDL. Both the value of the pseudo-continuum and the wavelength range used in the fit are varied to obtain the mean velocity of the feature along with the uncertainties in these measurements. Redshift uncertainties are also included in quadrature.

Foley, Sanders & Kirshner (2011) and Silverman, Kong & Filippenko (2012a) make independent calculations to correct Si II 6355 Å velocities to maximum light but find inconsistent relationships between velocity and phase. The relationships are also only accurate in a narrow light-curve width range, $1 < \Delta m_{15}(B)^4 < 1.5$ mag. Since some of our SNe Ia are not in this light-curve width range, we chose not to correct to maximum light and instead limit our analysis to a small phase range of -2 to $+5$ d with respect to maximum to minimize time-dependent variations. Not correcting the spectra to maximum light using the calculations of Silverman et al. (2012a) results in additional uncertainties of < 200 km s⁻¹ for our sample. For SNe Ia with spectra before and after maximum light (but limited to the range -5 to $+5$ d), we use a linear fit to estimate the value at maximum light. The Si II 6355 Å velocities are given in Table 3.

2.6 Na I D pseudo-equivalent-width measurements

The pseudo-equivalent width (pEW)⁵ of the narrow Na I D₂ absorption feature are also measured to investigate the potential contribution of CSM to the strength of the absorption. We use the Na I D₂

⁴ The decay of the B -band magnitude between maximum and 15 d post-maximum.

⁵ These are pEW and not true pEW since the continuum of a SN Ia spectrum is not a ‘true’ continuum but made up of many blended absorption lines.

feature since it is the stronger of the two Na I D lines. We calculate the pEW of the Na I D₂ components by first selecting the continuum on either side of the features of interest and then computing the area below the continuum, similar to the method of Förster et al. (2012). The pEW for the individual components are then totalled to provide an estimate of the pEW of the Na I D₂ line. This pEW measurement will contain contributions from host galaxy interstellar absorption, as well as potentially CSM from the SN progenitor system, if present.

2.7 Literature data

We supplement our SN Ia sample with events from the sample of Sternberg et al. (2011). They chose their high-resolution spectral sample to only include SNe Ia that were not specifically targeted due to either strong Na I D lines in classification spectra or showing red colours, which could be indicative of a CSM contribution, and which would have resulted in a biased sample. Since our data were similarly selected, we exclude other samples of high-resolution spectra if their selection criteria are not clearly outlined. This removes any potential bias from SNe Ia displaying positive detections of narrow absorption features being preferentially published.

We have collated photometric data from the literature for 16 of the 35 SNe Ia of Sternberg et al. (2011): SN 2006X, SN 2006cm, SN 2007af, SN 2007kk, SN 2009ds, SN 2009ig, SN 2010A from Hicken et al. (2009, 2012); SN 2007le, SN 2007on, SN 2008C, SN 2008fp, SN 2008hv, SN 2008ia from Stritzinger et al. (2011); SN 2008ec, SNF20080514-002 from Ganeshalingam et al. (2010); and SN 2009le from Maguire et al. (2012). The light-curve width and colour of these SNe were fit using SiFTO. The rest of the SNe Ia in the sample did not have well-constrained light-curve fits, due to sparse data coverage or poor data quality, or had stretch values outside the range used in cosmological studies ($0.7 < s < 1.3$).

We have gathered near-maximum light spectra of the following SNe Ia from the literature: SN 2006X (Wang et al. 2008), SN 2006cm, SN 2007le, SN 2007kk, SN 2008C, SNF20080514-002 (Blondin et al. 2012),⁶ SN 2007af (Simon et al. 2007; Blondin et al. 2012), SN 2009ig (Foley et al. 2012a) and SN 2009le (Maguire et al. 2012). Maximum light spectra of SN 2007on, SN 2008fp, SN 2008hv and SN 2008ia were obtained by the Carnegie Supernova Project (Phillips, private communication). This sample of 16 SNe Ia from Sternberg et al. (2011) with calculated light-curve parameters will be referred to as the S11 sample hereafter. The light-curve parameters and Si II 6355 Å velocities are given in Table A1.

3 ANALYSIS

We now turn to the analysis of our sample. We discuss first the definition of the zero velocity of the narrow absorption features, critical for defining relative velocity offsets. We then detail how the properties of the narrow absorption feature sample are dependent on host galaxy, light curve and spectral properties.

3.1 Spectral measurements of narrow absorption features

For our analysis of the XShooter spectra (Figs 1–3), we are interested in the position of the very narrow absorption features of Ca II

H&K and Na I D relative to a defined zero velocity (rest frame). These features do not originate from material in the SN ejecta, but rather from absorbing material along the line of sight, which can be caused by ISM in the host galaxy and/or CSM around the SN progenitor.

The frequency of occurrence of each type of profile with respect to a defined zero velocity (i.e. blueshifted, non-blueshifted or no absorption) can be measured, and the relative rates and possible correlations with other observables can then be determined. Hence, the definition of ‘zero velocity’ is critical, and can be set in a number of ways.

Previous studies, such as Sternberg et al. (2011) and Foley et al. (2012b), chose the strongest narrow Na I D absorption component as a proxy for the galaxy component at the SN position. ‘Blueshifted’, ‘redshifted’, ‘single/symmetric’ or ‘no absorption’ features are then determined relative to this position (see Sternberg et al. 2011, for further information). One disadvantage of this method is in cases where no host galaxy ISM absorption exists (perhaps more likely in early-type galaxies), SN Ia CSM features will then be misidentified as ‘single/symmetric’ even though they may originate from the SN environment itself.

Our method is to set the zero velocity relative to the positions of galaxy lines (e.g. narrow nebular emission lines of H α and H β) in the SN Ia spectrum. This probes the rest-frame velocity along the line of sight to the SN position. If these lines are not visible, the rest wavelength is instead set using the recessional velocity of the host galaxy, taken from the NASA/IPAC Extragalactic Database (NED) or SDSS. The advantage of this method is that ‘single/symmetric’ profiles can now be assigned a blueshifted or non-blueshifted position relative to the other host galaxy lines. The disadvantage is that using the recessional velocity does not account for any internal motion or rotation in the host galaxy. To estimate this potential offset for our SN Ia sample, we compare the SNe Ia that have a velocity measured from NED/SDSS and host galaxy lines in the spectra. The differences range from 20 km s^{−1} for SN 2013U to 150 km s^{−1} for SN 2012hd. When using the recessional velocities instead of host galaxy lines, one SN moves from being classified as ‘blueshifted’ to ‘non-blueshifted’ (SN 2012hd⁷). If the observed Na I D and Ca II H&K absorption features are all due to the host galaxy, one could expect an equal number of SNe Ia showing blueshifted and non-blueshifted absorption features. However, if there is an additional contribution to the blueshifted sample from the CSM, an excess of blueshifted features is expected. As this is a statistical argument, we do not discuss the CSM properties of individual SNe Ia in our sample. The zero-velocity positions of the S11 sample were also reanalysed for this study. The wavelength regions around their Na I D features were downloaded from WISEREP.

Previous studies have only identified time-varying blueshifted Na I D absorption features, while the Ca II H&K features have been found not to vary due to its higher ionization potential (Patat et al. 2007; Simon et al. 2009). Indeed, the non-detection of varying Ca II H&K is central to the argument for a CSM origin to the Na I D variations (see Patat et al. 2007, for detailed discussion). Therefore, we perform our analysis of velocity shifts of narrow absorption

⁶ Spectra obtained from the Weizmann Interactive Supernova data Repository (WiSeREP) – www.weizmann.ac.il/astrophysics/wiserep (Yaron & Gal-Yam 2012).

⁷ SN 2012hd has multiple Na I D and Ca II H&K absorption features that span a wide range of velocities. If the velocity of the SN progenitor system is assumed to be equal to that of the host galaxy emission lines then these features appear at both blueshifted and redshifted velocities, while if the recessional velocity of the host galaxy is used instead, all of the absorption features are redshifted.

features using the Na I D feature only. However, we show the Ca II H&K region in Figs 1–3, where it is seen that classification of the Na I D and Ca II H&K features (and relative velocities) agree for our XShooter sample for all but three SNe. The Ca II H&K region is also useful for confirming weak line detections at Na I D wavelengths.

We also searched for narrow K I absorption features. These features are expected to be much weaker than those of Ca II H&K and Na I D. SN 2012fw was the only SN in the sample to display K I absorption and showed non-blueshifted features, as did the Ca II H&K and Na I D absorption features for this event.

3.2 Defining the relative velocities

Having defined a zero-velocity position for each SN, we then search for absorption features near the zero velocities of the Na I D and Ca II H&K lines. We wish to extend the statistical analysis of Sternberg et al. (2011), and estimate the ratio of SNe Ia with blueshifted to redshifted Na I D absorption profiles in our sample. To do this, we classify our SN sample into five separate Na I D absorption categories: (i) SNe Ia with just blueshifted absorption, (ii) SNe Ia with just redshifted absorption, (iii) SNe Ia with blueshifted and redshifted features, (iv) SNe Ia with single absorption features at zero velocity and (v) SNe Ia with no Na I D absorption features. We split the sample in this way so that SNe Ia with only blueshifted Na I D absorption features can be directly compared to those with only redshifted Na I D absorption features, as was done in Sternberg et al. (2011).

The classifications of the Na I D features for both the XShooter sample and the combined sample with S11 are given in Table 4. Seven SNe show both blueshifted and redshifted features: SN 2006cm, SN 2007af, SN 2009ds, SN 2009le, SN 2010A, SN 2012cg, SN 2012hd, while LSQ12fuk is classified as symmetric since it shows only a single component at zero velocity with respect to $H\alpha$. The analysis of the ratio of SNe Ia in our sample with blueshifted to redshifted Na I D absorption features is detailed in Section 3.3.

For our analysis of the light-curve width and host galaxy properties as a function of Na I D absorption profile properties, we define our Na I D absorption categories by splitting the sample into three: (i) SNe Ia with any blueshifted absorption profiles ('blueshifted'), (ii) SNe Ia with only non-blueshifted absorption profiles ('non-blueshifted') and (iii) SNe Ia with no Na I D absorption features ('no absorption'). This different classification is made since SNe Ia with 'non-blueshifted' Na I D absorption features will always be associated with the host galaxy as they are not related to outflowing material and cannot be associated with the progenitor system. Conversely, SNe Ia displaying both blueshifted and redshifted Na I

D absorption features are now included in the 'blueshifted' category since any blueshifted Na I D absorption profiles seen *may* be associated with progenitor outflow – even though we cannot determine if this is the case for any individual SN. The breakdown of individual SNe Ia from our XShooter sample into these Na I D absorption categories is given in Section 3.1, while information on the SNe Ia from the S11 sample is given in Table A1.

In Section 3.6, we compare our colour and spectra analysis to those of Foley et al. (2012b), who split their sample into two categories, those that have blueshifted Na I D absorption features and those that do not ('everything else'). We also use these categories for investigating the pEW of Na I D features in Section 3.7, since we wish to determine if SNe Ia with blueshifted Na I D absorption features have stronger pEW than the rest of the sample.

3.3 Statistics of Na I D absorption profiles

Sternberg et al. (2011) identified an excess of blueshifted over redshifted Na I D absorption profiles in their SN Ia sample (12 SNe with 'blueshifted' features, 5 with 'redshifted' features, 5 with 'symmetric' profiles and 13 showing no narrow Na I D absorption features).

For the Xshooter sample alone, we find more SNe Ia showing blueshifted (five) Na I D absorption features compared to redshifted (two) Na I D absorption features (see Table 2 for the information on the individual SNe Ia and Table 4 for a summary of the total numbers in each grouping for this comparison.) Assuming an equal probability of obtaining a Na I D absorption profile that is 'blueshifted' or 'redshifted', we find a 16 per cent chance of this result occurring at random. For the combined sample, we also find more SNe Ia with only blueshifted Na I D absorption features (10) compared to only redshifted Na I D absorption features (4) for the combined sample, which has a 6 per cent chance of occurring at random. If equal numbers of the SNe Ia with blueshifted and redshifted Na I D absorption features are assumed to have a host galaxy ISM origin, this gives an excess of seven SNe Ia with anomalous blueshifted Na I D features. This is equivalent to 19 per cent of the total sample of 32 SNe Ia having an additional blueshifted component.

For comparison, we also use the original method of Sternberg et al. (2011) for our combined sample (where the strongest component is chosen as the velocity zero-point) and find 14 SNe with blueshifted features, 4 SNe with redshifted features, 4 with symmetric features and 10 with no absorption features – again showing an excess of blueshifted over redshifted features (~30 per cent of the sample) with 1.2 per cent chance occurrence probability.

3.4 Host galaxy distribution

Fig. 4 shows the morphological-type distribution for the combined sample of our data and the S11 sample, split into those that show blueshifted (any SN Ia showing any blueshifted Na I D features), non-blueshifted (containing only 'non-blueshifted' absorption features) or no Na I D absorption features. PTF12jgb is excluded here because its galaxy morphology could not be determined. The galaxy categories are 'E', 'S0', 'Sab', 'Sbc', 'Sc/Scd' and 'Irregular/Dwarf'. The host galaxies of two SNe Ia in the sample are categorised as S0/a (SN 2012fw, SN 2008fp). We classify them half each in the 'S0' and 'Sa' bins but because they are both classified as 'non-blueshifted' this does not result in non-integer values in Fig. 4.

We find that SNe Ia with detected narrow Na I D absorption features are found more frequently in late-type galaxies, as has been found in previous studies (Foley et al. 2012b; Förster et al. 2013). This is expected as star-forming galaxies typically contain

Table 4. Classification of Na I D features for XShooter sample and combined sample with S11.

Na I D classification	XShooter sample	Combined sample
Blueshifted only	5	10
Redshifted only	2	4
Blue and Redshifted	2	7
Symmetric	1	1
None	6	10
Excess of blueshifted ^a	19 per cent	19 per cent
Total	16	32

^aExcess of SNe Ia with only blueshifted Na I D absorption features compared to only redshifted Na I D absorption as a percentage of the total sample.

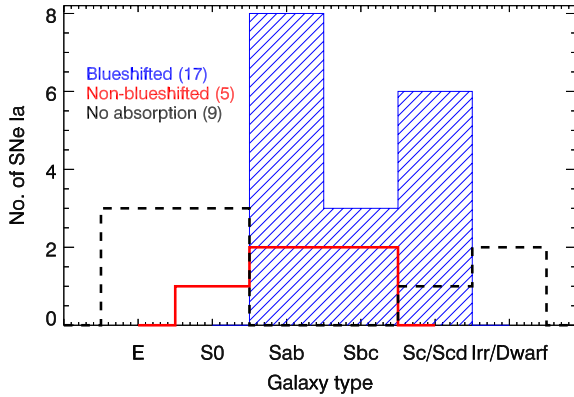


Figure 4. Histogram of the host galaxy types of 31 SNe Ia from the combined S11 sample and our XShooter sample, split into SNe Ia showing any blueshifted Na I D features including those showing both blueshifted and non-blueshifted features (‘blueshifted’; blue hashed region), only non-blueshifted Na I D absorption features (‘non-blueshifted’; red solid line) or no Na I D absorption features (‘no absorption’; black dashed line).

denser ISM. Conversely, the SNe Ia displaying no Na I D features are predominantly found in early-type host galaxies. No SN Ia with blueshifted Na I D features in our sample is found in an early-type galaxy (E/S0) compared to 17 ‘blueshifted’ SNe Ia in late-type hosts. From Section 3.3, we estimate that ~ 11 of the SNe Ia displaying blueshifted Na I D features are caused by CSM, with the remaining ~ 6 due to ISM.⁸ However, we cannot determine which SNe Ia fall into which category since we do not have the necessary information for any individual event. For the two SNe in elliptical host galaxies, neither show narrow Na I D absorption features.

3.5 Light-curve width

Given the excess of blueshifted SNe Ia in late-type galaxies, the lack of blueshifted SNe Ia in early-type hosts, and the well-studied connection between light-curve width and host galaxy properties (SNe Ia in late-type galaxies having broader light curves or higher ‘stretch’ than those in early-type galaxies; Hamuy et al. 1995, 1996, 2000; Riess et al. 1999), we wish to investigate potential correlations between the presence of blueshifted Na I D absorption profiles and SN Ia luminosity (using light-curve width as a proxy).

Fig. 5 shows a histogram of the light-curve width parameter, ‘stretch’, for our SN sample, colour-coded based on the presence of blueshifted Na I D absorption features, ‘non-blueshifted’ absorption features or no Na I D absorption. SNe Ia displaying Na I D absorption features have, on average, broader light curves than those with no Na I D absorption. A Kolmogorov–Smirnov (K-S) test shows that there is a high probability (p -value = 0.015) that the ‘blueshifted’ and ‘non-blueshifted’ stretch distributions are drawn from a different parent population to the ‘no absorption’ sample’s stretch distribution. This is not surprising since the SNe Ia with no Na I D absorption are located preferentially in early-type galaxies, where SNe Ia are well known to have narrower light curves than those

⁸ If equal numbers of the SNe Ia with blueshifted and redshifted only Na I D absorption features are assumed to have a host galaxy ISM origin, then four out of the 11 showing blueshifted only Na I D features should be due to ISM, which is ~ 36 per cent. Then, 36 per cent of the 17 SNe Ia showing ‘blueshifted only’ or ‘blueshifted and redshifted’ features is equal to 6 SNe Ia in the combined ‘blueshifted’ sample having features due to ISM, with the rest (11 SNe Ia) caused by CSM.

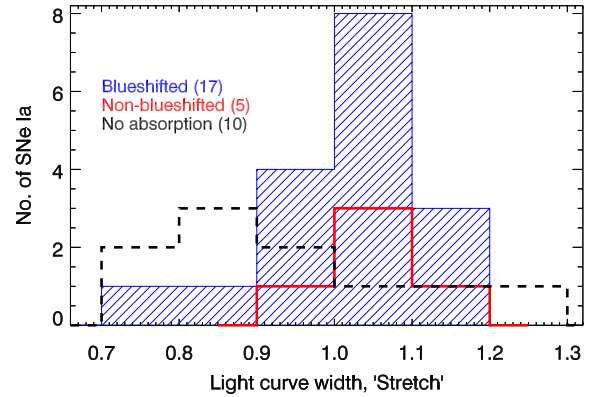


Figure 5. Histogram of the light-curve width parameter, ‘stretch’, colour-coded depending on the presence of blueshifted Na I D absorption features (blue hashed region), non-blueshifted Na I D absorption features (red solid line) or no Na I D absorption (black dashed line).

in later-type host galaxies. We note that any K-S test probability involving the ‘blueshifted’ sample is actually a lower limit, since we expect that ~ 6 SNe Ia in the ‘blueshifted’ sample are not due to ISM (not CSM) in the host galaxy and therefore, contaminate the ‘blueshifted’ population.

Within the sub-sample of SNe Ia showing non-zero Na I D absorption features, we find a low probability of the ‘blueshifted’ and ‘non-blueshifted’ stretch distributions being drawn from different parent populations, with both samples displaying broader light curves, and occurring more frequently in late-type galaxies than those with no Na I D absorption features.

3.6 SN colour and Si II 6355 Å velocity

Claims that SNe Ia displaying blueshifted Na I D absorption features have redder optical colours ($B_{\max} - V_{\max}$ pseudo-colour⁹) and having increased Si II 6355 Å line velocities than the rest of the SN Ia population have been made (Foley et al. 2012b). First, we investigate the relationship between SN colour and blueshifted Na I D features. We choose to study the $B - V$ colour at the time of B -band maximum since it is a more physical quantity than $B_{\max} - V_{\max}$ pseudo-colour. However, the two quantities are strongly correlated (Blondin et al. 2012) and our choice does not affect the results.

To make a suitable comparison to Foley et al. (2012b), we group the SNe Ia in our sample into those displaying blueshifted Na I D (‘blueshifted’) and those that do not, including both those that show non-blueshifted Na I D absorption and those with no absorption features (‘everything else’). In Fig. 6, we show the $B - V$ colour distributions for the full SN Ia sample. A K-S test for the samples gives a p -value of 0.10 that the ‘blueshifted’ and ‘everything else’ samples are drawn from different parent $B - V$ colour populations, which is larger than the typically used significance level of < 0.05 . Any difference is primarily driven by a single object SN 2006X, which had an unusually red $B - V$ colour of 1.22 ± 0.01 , making it an outlier to the SN population as a whole.

The connection between Si II 6355 Å velocity and blueshifted Na I D absorption profiles is also investigated. Fig. 7 shows the maximum light Si II 6355 Å velocity as a function of stretch for both the ‘blueshifted’ and ‘everything else’ samples. Using a K-S test,

⁹ B -band magnitude at B maximum minus V magnitude at V -band maximum.

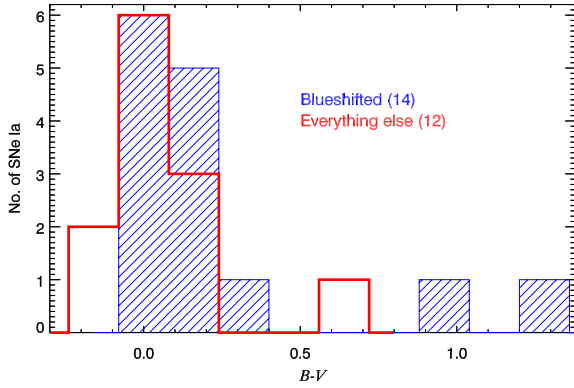


Figure 6. $B - V$ colour distribution of the SN Ia sample in all galaxy types, colour-coded based on the presence of blueshifted Na I D absorption features (blue hashed) or absence ('everything else', red line). The bin size of 0.16 is chosen as twice the largest uncertainty on a colour measurement. The numbers in parentheses indicate the number of SNe Ia in each Na I D group.

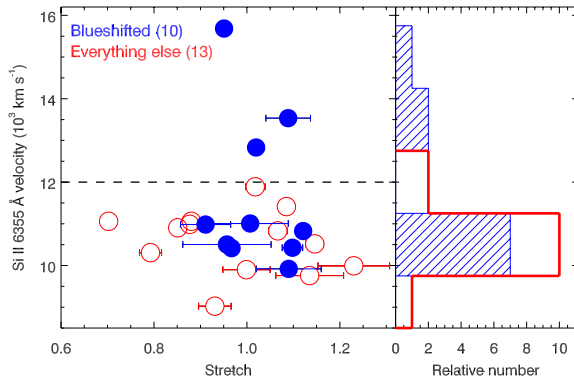


Figure 7. The Si II 6355 Å velocity around maximum light is shown against the light-curve width parameter, stretch. The SNe are colour-coded based on the presence (blue, solid circles) or absence (red, open circles) of blueshifted Na I D absorption profiles. The uncertainties on the velocity measurements are smaller than the symbols. The dashed horizontal line marks the lower limit for 'high-velocity' SNe Ia as defined by Wang et al. (2013) of 12 000 km s⁻¹.

we find a very low probability (p -value=0.7) that the 'blueshifted' and 'everything else' samples are drawn from different parent Si II velocity distributions. We note that the three SNe Ia (SN 2006X, SN 2007le, SN 2009ig) with the highest Si II 6355 Å velocities do show blueshifted Na I D features and fall in the 'high-velocity' (HV) class of SNe Ia (Wang et al. 2009), defined as having a Si II 6355 Å velocity of $>12\,000$ km s⁻¹. However, the velocity distribution of the blueshifted sample does not show a statistically significant difference from the rest of our SN Ia sample.

3.7 Relative strength of Na I D absorption components

The pEW of the Na I D features can be used to estimate the relative amount of absorbing material along the line of sight towards the SNe in the sample. We do not attempt to convert these values to column densities but perform a relative comparison between SNe Ia in our sample showing blueshifted material and the 'everything else' sample as defined in Section 3.6.

Fig. 8 shows the sum of the pEW of Na I D₂ components for each SN Ia split based on the presence or absence of blueshifted Na I D absorption profiles. The Na I D₂ pEW values are given in Table 2

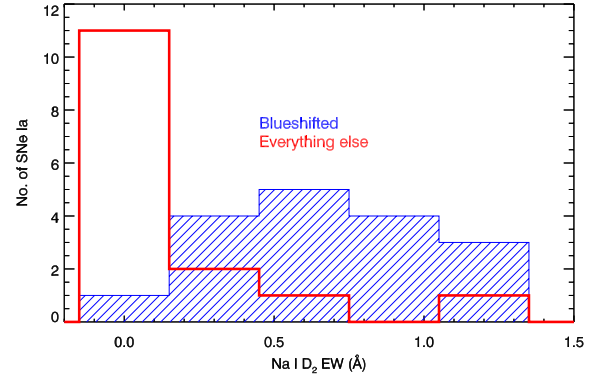


Figure 8. Histogram of the pEW of the narrow Na I D₂ features of the SN Ia sample for all SNe in the sample, colour-coded depending on the presence (blue hashed) or absence (red line) of blueshifted Na I D absorption features.

for the XShooter sample and in Table A1 for the S11 sample. We find that SNe Ia with blueshifted Na I D absorption features have higher Na I D₂ pEW values than those without blueshifted Na I D absorption features. A K-S test gives a very high probability (p -value=0.0004) of the 'blueshifted' and 'everything else' Na I D₂ pEW distributions being drawn from different parent populations.

These higher Na I D₂ pEW in the 'blueshifted' sample may potentially be explained by an additional contribution from CSM to their strength. To investigate the origin of this additional contribution further, we measure the integrated pEW of only the 'blueshifted' Na I D₂ components (excluding any non-blueshifted components) in the 'blueshifted' SN Ia sample. The 'blueshifted' Na I D₂ pEW is then defined as the pEW of any features (fractional or full) that are blueshifted with respect to our defined zero velocity.

The left-hand panel of Fig. 9 shows the $B - V$ colour at maximum as a function of the pEW of their 'blueshifted' Na I D₂ features. Two SNe Ia in the sample (SN 2006X, SN 2006cm) are found to lie nearly 6σ away from the mean $B - V$ colour of the sample and off the identified relation between Na I D₂ pEW and $B - V$ colour at maximum, suggesting a strong contribution from dust in the galaxy to their $B - V$ colour. Excluding these reddened events, we find a strong correlation between the $B - V$ colour at maximum and the 'blueshifted' Na I D₂ features at the 5.7 σ level.

We also investigate the stretch and Si II 6355 Å velocity at maximum as a function of 'blueshifted' Na I D₂ pEW (also shown in Fig. 9). No statistically significant correlations between either Si II 6355 Å velocity or stretch and 'blueshifted' Na I D₂ pEW is found.

4 DISCUSSION

We have presented a new SN Ia spectral sample exploring the connection between the narrow absorption lines of Ca II H&K and Na I D in SN Ia spectra and the photometric and spectral properties of SNe Ia. We now discuss the interpretation of these results in the context of SN Ia progenitor channels, as well as highlight the increasing evidence for distinct families of SNe Ia.

4.1 CSM and SN Ia progenitor scenarios

Time-varying blueshifted narrow Na I D absorption features have been identified in some SNe Ia (e.g. Patat et al. 2007; Blondin et al. 2009; Simon et al. 2009; Stritzinger et al. 2010), with the suggestion that these varying profiles are related to outflowing material from their progenitor systems. The velocities of this outflowing material

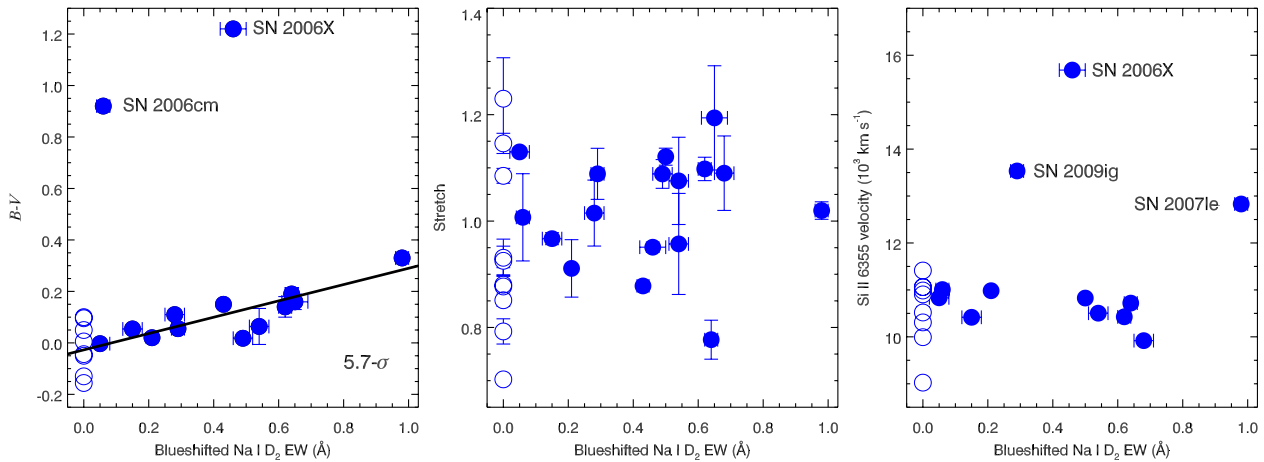


Figure 9. Left: the $B - V$ colour at maximum as a function of the pEW of the ‘blueshifted’ only narrow Na I D₂ features for the SNe Ia in our sample displaying ‘blueshifted’ features. The solid blue circles represent positive detections of ‘blueshifted’ narrow Na I D₂ features, while the open circles represent non-detections. SN 2006X and SN 2006cm are extreme outliers to the colour relation and have been excluded from the fit. The solid black line is the best linear fit to the data, with a significance of 5.7σ . Middle: the stretch of the SNe Ia as a function of the pEW of the ‘blueshifted’ only narrow Na I D₂ features for the SNe Ia in our sample displaying ‘blueshifted’ features. No correlation is identified. Right: the Si II 6355 Å velocity against the pEW of the ‘blueshifted’ only narrow Na I D₂ features. The three SNe Ia falling in the ‘HV’ group of Wang et al. (2013) are labelled. No correlation is identified.

with respect to the defined rest frame of the SNe are typically ~ 50 – 200 km s^{-1} , while the distances to the absorbing material have been estimated to be 10^{16} – 10^{17} cm and having cloud densities of 10^7 cm^{-3} (Patat et al. 2007; Simon et al. 2009). Patat et al. (2011) showed that the recurrent nova system, RS Ophiuchi (RS Oph), showed very similar time-variable Na I D absorption features during outburst, to those observed in SN 2006X, suggesting a strong connection between recurrent novae and SNe Ia that show time-variable Na I D absorption features. Three-dimensional modelling of RS Oph has shown that the CSM is expected to be concentrated in the binary orbital plane, suggesting that the probability of detecting CSM is also strongly dependent on viewing angle (Mohamed, Booth & Podsiadlowski 2013).

Regions of very recent star formation ($< 100 \text{ Myr}$) have been found to have outflows with velocities of ~ 100 – 200 km s^{-1} (van Loon et al. 2013), similar to those seen in our SN Ia sample. However, SNe Ia are not preferentially found near these regions of recent star formation and therefore, should not be related to these regions of outflowing material – even the so-called prompt SNe Ia that trace the host galaxy star formation rate occur on time-scales of at least 200 Myr (Raskin et al. 2009).

A statistical study of a sample of single-epoch high-resolution spectra of SNe Ia was performed by Sternberg et al. (2011), where an excess of SNe Ia displaying blueshifted Na I D absorption features compared to non-blueshifted Na I absorption features in spiral galaxies was found. This was interpreted as evidence favouring the SD progenitor channel for some SNe Ia in spiral galaxies.

In our sample, we find an excess of SNe Ia displaying blueshifted Na I D absorption features compared to those that show non-blueshifted absorption features, with an estimate of ~ 20 per cent of SNe Ia showing additional blueshifted Na I D absorption features. This value is most likely a lower limit since the CSM distribution is expected to be asymmetric, resulting in cases where CSM is present but not seen due to the viewing angle. We also show that the presence of Na I D absorption features is strongly dependent on host galaxy properties with SNe Ia displaying blueshifted features predominantly found in later-type galaxies. No SN Ia with blueshifted Na I D features is found in an early-type (E/S0) galaxy.

Although Na I D and Ca II H&K absorption lines arising from within the host galaxies are expected to be stronger in late-type galaxies, there is no simple ‘host galaxy’ explanation for the observed excess of ‘blueshifted’ narrow absorption components.

We also find that the strength of Na I D absorption features is correlated with the presence or absence of blueshifted Na I D absorption features – SNe Ia with blueshifted Na I D absorption features have stronger Na I D lines (measured through the pEW of the stronger of the two Na I D lines, Na I D₂) than SNe Ia that do not have blueshifted Na I D features. This increased Na I D absorption depth in SNe Ia showing ‘blueshifted’ material, coupled with the identified excess of SNe Ia with ‘blueshifted’ SNe Ia, is strongly suggestive of an additional contribution to the Na I D absorption from the SN progenitor system.

SNe Ia displaying no Na I D absorption features have been found to have narrower light curves than those that show ‘blueshifted’ Na I D absorption features (Foley et al. 2012b). Our data suggest that SNe Ia showing Na I D absorption features (both ‘blueshifted’ and ‘non-blueshifted’) have broader light curves than those that do not show Na I D absorption features. However, interestingly we find no correlation between the pEW strength of ‘blueshifted’ Na I D₂ features and the light-curve width, suggesting that once we look within the sample of SNe Ia with ‘blueshifted’ Na I D₂ features, there is no additional relation between Na I D strength and light-curve width. These results appear to be linked to the host galaxy distribution of the sample – SNe Ia with Na I D absorption features are predominantly found in late-type host galaxies, where it is well known that the SNe Ia display broader light curves (Hamuy et al. 1995, 1996, 2000; Riess et al. 1999). However, it is still difficult to identify the driving force behind these correlations since the reason why less luminous SNe Ia preferentially occur in early-type galaxies compared to late-type galaxies is not well understood.

SNe Ia with blueshifted Na I D absorption features have previously been suggested to have redder $B - V$ colours at maximum and higher Si II 6355 Å velocities compared to the SN Ia population as a whole (Foley et al. 2012b). The three SNe Ia in our combined sample with the highest velocities ($> 12000 \text{ km s}^{-1}$), and falling in the ‘high-velocity’ class of Wang et al. (2009), do display

blueshifted absorption features, and the two reddest SNe Ia in the sample display blueshifted Na I D features. However, for our sample, we find no statistically significant difference between the velocity and colour of the SN Ia sample when split into those with blueshifted Na I D absorption profiles and those without. We also find that these differences are primarily driven by SN 2006X, a very red outlier with high Si II velocities, which has blueshifted Na I D absorption features. The highly interacting SN Ia, PTF11kx, which displayed very strong H in its spectra, as well as time-varying Na I D absorption, had a relatively low Si II 6355 Å velocity at maximum of $\sim 11\,000\text{ km s}^{-1}$, which does not suggest a continuing trend of higher velocities towards more highly interacting SNe Ia. We also find no correlation between Si II 6355 Å velocity at maximum and the strength (pEW) of ‘blueshifted’ Na I D absorption features.

For completeness, we note that none of the SNe Ia with ‘HV’ Si II features are from the new XShooter sample nor does the XShooter sample contain any SN Ia with a red $B - V$ colours that would exceed the colour cut-off used in SN Ia cosmological studies of 0.25, while the S11 sample contains four. However, we do not find a statistically significant difference between the XShooter and S11 colour or Si II velocity distributions.

When we study the connection between the pEW of ‘blueshifted’ Na I D₂ features (pEW of features blueshifted with respect to the zero velocity) and the SN $B - V$ colour at maximum light, we find a strong correlation (5.7σ). An obvious explanation for SNe Ia with stronger ‘blueshifted’ Na I D pEW having redder colours is that dust in the CSM makes an additional contribution to the extinction towards the SN resulting in a redder $B - V$ colour. The effect of circumstellar dust on the $B - V$ colour and the effective extinction law has been previously modelled (Goobar 2008; Amanullah & Goobar 2011). It has been found that dust in the CSM could cause $B - V$ colour variations are of the order of 0.05–0.1 mag for dust radii of 10^{16} – 10^{19} cm.

Förster et al. (2013) have recently shown that SNe Ia that are faster Lira law $B - V$ decliners (35–80 d after maximum) have higher pEW values of unresolved Na I D absorption features (measured from lower resolution spectra) and redder colours at maximum than slower Lira law $B - V$ decliners. They attribute this difference as evidence of CSM in the ‘fast decliner’ group. A direct comparison with their results cannot be made since their study uses lower resolution spectra, and therefore, information on the relative velocity shifts and strength of the ‘blueshifted’ Na I D features is not available.

4.2 CSM from DD channels

Some recent work has attempted to explain the observations of outflowing CSM material using a DD origin. Shen et al. (2013) showed that the interaction between material ejected from a He–CO WD binary system and the ISM could produce outflowing neutral Na. In agreement with our results, they also found that the lower ISM densities in elliptical galaxies would inhibit detection of blueshifted absorption features in these galaxies. Raskin & Kasen (2013) showed that tidal tails from DD WD mergers interacting with the ISM may also produce outflowing material that could result in observed blueshifted absorption features. Additional analysis and simulations are necessary to quantify the absorbing material that would be present and to explore the exact conditions of the CSM and ISM that are needed to produce the observed features and correlations with SN properties.

Models of the violent merger of a WD with the core of a giant star during the common envelope phase can also explain the

Table 5. Observational evidence for two families of SNe Ia.

Family 1	Family 2	Ref.
More luminous	Less luminous	1
Broad light curve	Narrow light curve	1
Low Si II 4130 pEW	High Si II 4130 pEW	2
Stronger high-velocity features	Weaker high-velocity features	3
Late-type host	Early-type host	4
Low M_{stellar} host	High M_{stellar} host	5
High sSFR host	Low sSFR host	6
Short delay-time	Long delay-time	7
Blueshifted Na I D absorption	No Na I D absorption	This paper

1 – Phillips (1993)

2 – Bronder et al. (2008); Arsenijevic et al. (2008); Walker et al. (2011), Blondin, Mandel & Kirshner (2011), Chotard et al. (2011); Blondin et al. (2012); Silverman et al. (2012b)

3 – Maguire et al. (2012); Childress et al. (2013b)

4 – Hamuy et al. (1995, 1996, 2000); Riess et al. (1999)

5 – Sullivan et al. (2010)

6 – Gallagher et al. (2005); Sullivan et al. (2006)

7 – Mannucci et al. (2005), Mannucci, Della Valle & Panagia (2006), Scannapieco & Bildsten (2005); Sullivan et al. (2006); Smith et al. (2012); Childress et al. (2013a)

presence of CSM (Soker et al. 2013). Population synthesis modelling has suggested that some SNe Ia produced from violent CO+CO WD mergers may show signs of CSM if the SN Ia explodes soon after the common envelope phase (< 1000 yr), although the rate of these events is expected to be low (< 4 per cent; Ruiter et al. 2013). Models of canonical CO+CO WD mergers require delay times of 10^5 yr between the initial dynamical merger and the explosion, effectively ruling out this CSM production mechanism in non-violet WD mergers (Yoon, Podsiadlowski & Rosswog 2007). Therefore, it seems unlikely that this channel can fully explain the rates of blueshifted Na I D absorption features that have been observed.

4.3 Evidence for two (or more) families of SNe Ia?

The observed connection between the presence (and strength) of narrow blueshifted Na I D absorption features in SN spectra and observed SN properties has a number of implications, independent of the exact progenitor configuration. The clear excess of SNe Ia in our sample displaying blueshifted Na I D absorption compared to those with non-blueshifted Na I D absorption suggests an additional contribution from CSM to the absorption profiles. SNe Ia with wider light curves have long been known to be intrinsically more luminous (Phillips 1993), but many other SN properties are also connected to light-curve width.

In Table 5, we show the observed SN Ia properties that are found to be related to SN Ia luminosity. As well as broader light curves ($s > 1.0$),¹⁰ more luminous SNe Ia also have lower Si II 4130 Å pEW than less luminous SNe Ia (Arsenijevic et al. 2008; Bronder et al. 2008; Walker et al. 2011; Blondin et al. 2011, 2012; Chotard et al. 2011).

Trends of some SN spectral feature velocities increasing with increasing light-curve width have previously been identified (e.g.

¹⁰ The position of the split between low and high stretch is made based on the mean stretch value of the SNLS SN Ia sample ($s = 1.0$) from Guy et al. (2010).

Wells et al. 1994; Fisher et al. 1995; Mazzali et al. 2007; Maguire et al. 2012) – higher Ca II H&K and Ca II near-infrared (NIR) velocities at maximum are associated with SNe Ia with broader light-curve widths. One possible cause for these correlations is a stronger contribution from ‘high-velocity’ material in more luminous SNe Ia (Maguire et al. 2012). Childress et al. (2013b) have identified a connection between the strength of ‘high-velocity’ features in SNe Ia spectra and light-curve width, with more luminous SNe Ia displaying stronger ‘high-velocity’ components in the Ca II NIR feature. One suggested mechanism for ‘high-velocity’ features is a density enhancement at high velocity, either from CSM (i.e. a ‘detached shell’ of material) or intrinsic to the SN (Mazzali et al. 2005; Blondin et al. 2012).

The photometric properties of SNe Ia are also closely linked to their host galaxy properties. SNe Ia in morphologically elliptical systems are intrinsically fainter and lower stretch than SNe Ia in spiral or late-type galaxies (Hamuy et al. 1995, 1996, 2000; Riess et al. 1999). These correlations also apply when examining physical variables, which define the stellar populations of the SN hosts instead of morphology, with more luminous, higher stretch SNe Ia in less massive galaxies (Sullivan et al. 2010) and more strongly star-forming galaxies (Gallagher et al. 2005; Sullivan et al. 2006) than less luminous (lower stretch) SNe Ia. Thus, high stretch SNe Ia seem to favour younger stellar environments and thus likely younger progenitor systems. X-rays signatures of accreting WD systems in early-type galaxies have also been found to be rare with Gilfanov & Bogdán (2010) suggesting that no more than 5 per cent of SNe Ia in early-type galaxies can come from the SD channel (although see Meng & Yang 2011; Kato 2013).

Direct measurements of the SN Ia host galaxy ages, although very challenging, also support a relation between stretch and galaxy age (Johansson et al. 2013; Pan et al., in preparation). This is supported by studies of the SN Ia delay-time distribution (DTD); when the DTD is constructed for low and high stretch events, again higher stretch SNe favour a younger DTD (Brandt et al. 2010; Maoz, Mannucci & Brandt 2012). SN Ia rates have also been found to depend on both host galaxy star formation rate and host stellar mass, leading to the idea of a two-component model for SNe Ia, with both ‘prompt’ (<500 Myr) and ‘delayed’ (>500 Myr) channels acting to produce SNe Ia (Mannucci et al. 2005, 2006; Scannapieco & Bildsten 2005; Sullivan et al. 2006; Smith et al. 2012; Childress et al. 2013a).

Wang et al. (2013) have suggested a connection between the Si II 6355 Å velocity at maximum and the location of SNe Ia in their host galaxies – more centrally located SNe Ia display, on average, higher Si II 6355 Å velocities, suggested to be linked to a younger stellar population. However, they find no connection between Si II 6355 Å velocity and light-curve width, which may be expected given the previously identified links between younger stellar populations and higher SN luminosity.

SN Ia remnants also show diversity in their properties with Galactic SN remnants such as Tycho showing no signs of interaction with CSM (Badenes et al. 2006), while searches for a non-degenerate companion star for Tycho have not identified a companion star consistent with its expected properties (Kerzendorf et al. 2013). However, *Kepler*’s SN remnant, which has been shown to be an overluminous SN Ia (Patnaude et al. 2012), displays signatures of interaction between the SN ejecta and CSM (e.g. Dennefeld 1982; Bandiera 1987; Burke et al. 2013), as well as strong evidence for supersolar metallicity of the progenitor (Park et al. 2013) and warm dust originating from swept-up CSM (Gomez et al. 2012). These properties are consistent with the explosion of a SN Ia through a rel-

atively prompt progenitor channel, while Tycho is more consistent with an older progenitor.

The connection between SN luminosity and SN observables presented in Table 5 is suggestive of a split in SNe Ia properties based on their luminosity, which correlates with many observed SN Ia properties. Within ‘Family 1’, we have further identified a trends between SN $B - V$ colour at maximum and pEW of the ‘blueshifted’ Na I D absorption features, suggestive of an increasing contribution from CSM leading to an increasing contribution from dust.

However, it is still unclear what the driving force behind these correlations is and whether they are directly linked to independent progenitor channels. Any viable progenitor model must be able to explain this observed diversity in SN Ia properties. Our estimate is that at least 20 per cent of SNe Ia have an additional contribution from CSM as measured from the excess of ‘blueshifted’ Na I D absorption features, as well as their stronger Na I D pEW than the rest of the SN Ia sample. We interpret this percentage as a lower limit since any asymmetry in the CSM (i.e. a concentration in the binary orbital plane as shown in RS Oph; Mohamed et al. 2013) will result in line-of-sight effects, where outflowing CSM is present but not observed.

4.3.1 Type Ia-CSM SNe

For ‘normal’ SNe Ia the detection of H in their spectra is a key diagnostic of the SD progenitor channel, since the origin of this H is most likely from a non-degenerate companion star. This detection of hydrogen lines had, until recently, only been confirmed for a handful of events: SN 2002ic (Hamuy et al. 2003; Deng et al. 2004; Kotak et al. 2004; Wang et al. 2004; Wood-Vasey, Wang & Aldering 2004), SN 2005gj (Aldering et al. 2006; Prieto et al. 2007), SN 2008J (Taddia et al. 2012) and PTF11kx (Dilday et al. 2012). These objects are interacting with their CSM to an even stronger degree than the SNe studied here, with strong narrow hydrogen emission, and have recently been dubbed ‘SNe Ia-CSM’ (Silverman et al. 2013). These authors conducted a detailed search in the spectra of SNe classified as IIn from PTF and the literature, for diluted signatures of SNe Ia, and found a total of 16 Ia-CSM objects.

The most common SN Ia template spectrum for the SNe Ia-CSM was suggested by Silverman et al. (2013) to be, the brighter than average, 1991T/1999aa-like spectrum. However, it is only with model spectral templates that this has been shown not to be a luminosity bias (Leloudas et al. 2013). While SN 1991T itself did not show the narrow emission lines typical of SNe Ia-CSM and IIn, it did display blueshifted Na I D absorption features (Patat et al. 2007), suggesting an association between SN 1991T and the more luminous than average SNe Ia that show strong signatures of CSM interaction.

In some respects, events in this SN Ia-CSM class may represent a more extreme version of the objects observed here, and are also preferentially located in late-type spirals or dwarf irregulars, star-forming galaxies similar to the hosts of our blueshifted Na I D absorption feature objects.

4.3.2 The search for H in late-time spectra

Even for SN Ia events without a dense enough CSM to produce hydrogen in the photospheric spectra, hydrogen-rich material may still be stripped from the companion star by the SN ejecta. This hydrogen is then predicted to be present at low velocities ($\sim 1000 \text{ km s}^{-1}$) and can only be detected after the outer (higher velocity) layers have become optically thin (Marietta, Burrows & Fryxell 2000; Meng, Chen & Han 2007). A search for this hydrogen has been conducted in five

‘normal’ SNe Ia at the necessary late times (SN 2001el, SN 2005am, SN 2005cf, SN 2011fe, SN 1998bu), but none has yet been detected, with a mass limit of the hydrogen of $<0.03 M_{\odot}$ ($<0.001 M_{\odot}$ for nearby SN 2011fe), disfavouring a SD progenitor channel (Mattila et al. 2005; Leonard 2007; Lundqvist et al. 2013; Shappee et al. 2013). However, some models predict that the companion star will have lost its envelope by the time of explosion, providing an alternative explanation for the absence of H features in SNe Ia (Di Stefano, Voss & Claeys 2011; Justham 2011).

However, these SNe Ia have stretches of 0.99 ± 0.01 (SN 2001el), 0.96 ± 0.01 (SN 2005cf), 0.70 ± 0.03 (SN 2005am), $0.96 \sim 0.02$ (SN 1998bu) and 0.98 ± 0.01 (SN 2011fe), placing them all in the lower stretch family ($s < 1.01$). If the hypothesis that this lower luminosity family comes from an older stellar population such as through the DD progenitor channel, we do not expect to see hydrogen in their late-time spectra. A search for hydrogen in the spectra of higher stretch SNe Ia would therefore be an interesting study.

4.3.3 Individual case studies

Finally, we discuss two well-studied SNe Ia from our sample to determine which column of Table 5 they most likely fit into. However, we stress that since some SNe Ia show blueshifted Na I D absorption features associated with host galaxy ISM and not CSM, it is not necessary that individual objects will fall completely into either class.

SN 2011fe exploded in M101, a high stellar mass galaxy (Nugent et al. 2011). Its light-curve stretch of 0.98 and lower spectral velocities place it in Family 2. Despite extensive monitoring, no CSM was detected in high-resolution spectra. Pre-explosion imaging has ruled out more massive companion progenitor stars, favouring a low-mass or degenerate companion star (Li et al. 2011). As discussed in Section 4.3.2, no H was detected in its late-time spectra with an upper mass limit of $<0.001 M_{\odot}$.

SN 2012cg was a nearby (~ 15 Mpc) SN Ia discovered just 1.5 ± 0.2 d after explosion. It had a stretch of 1.098 ± 0.022 , occurred in a barred Sa galaxy [typically low stellar mass, high specific Star Formation Rate (sSFR)] and displayed blueshifted narrow absorption features of Ca II H&K and Na I D. These characteristics place it in Family 1 of Table 5.

5 CONCLUSIONS

In this paper, we have presented a sample of 17 low-redshift SNe Ia observed with the XShooter intermediate-resolution spectrograph on the VLT. We conducted a search for narrow Na I D absorption profiles in these spectra and, where present, have measured its blueshift (or non-blueshift) relative to the systemic velocity of the SN in its host galaxy. We combined these new data with events from the literature to form a single sample of 32 SNe Ia with intermediate-high resolution spectra and light-curve data. We also measured the strength of the narrow Na I D absorption features through pEW measurements and investigated the connection to SN observables. Our main conclusions are as follows.

- (i) Combining our new data with the S11 sample, we find an excess of SNe Ia with blueshifted Na I D absorption features over those with redshifted Na I D, with ~ 20 per cent of SNe Ia having an additional blueshifted Na I D absorption feature.
- (ii) SNe Ia with Na I D absorption features in their spectra have, on average, broader light curves (or higher stretches) and are more luminous events than SNe Ia without Na I D absorption features.

- (iii) SNe Ia with blueshifted Na I D absorption features are most likely to be found in late-type galaxies containing younger stellar populations. No SNe Ia in our sample with blueshifted Na I D were found in an E/S0 galaxy.

- (iv) SNe Ia with blueshifted Na I D absorption features show stronger Na I D pEWs than those without blueshifted features, suggestive of an additional contribution to the Na I D absorption from CSM.

- (v) Within the sample of SNe Ia with blueshifted Na I D absorption, we find that the strength of the ‘blueshifted’ Na I D absorption features correlates with SN $B - V$ colour at maximum, strongly suggesting this material is associated with the progenitor system.

- (vi) We find no statistically significant preference for SNe Ia with blueshifted Na I D features to have higher Si II 6355 Å velocities than SNe Ia without blueshifted Na I D features.

The simplest explanation for the presence of additional blueshifted Na I D absorption features in SN Ia spectra is that it arises due to CSM from the progenitor system of the SN. This suggests a progenitor channel where one would expect outflowing shell-like structures – the most obvious being the SD scenario. A SD origin for the CSM is supported by clear observational evidence with recurrent nova systems being observed to show time-varying Na I D features very similar to those in some SNe Ia. However, some recent DD models may now also produce similar narrow absorption features, but not currently at the rate necessary to explain our results.

Table 5 summarizes the observational evidence for two distinct families of ‘normal’ SNe Ia with different light curve, spectral and host galaxy properties. The rates of the different channels are consistent with one population with high luminosity, short delay-times and evidence for outflowing material, with the other population displaying no Na I D absorption features, low luminosity and long delay-times indicative of an older population. Whether these ‘families’ correspond to separate progenitor channels (SD and DD) or can be explained within the framework of one channel (i.e. different types of companion stars in the SD channel) is still very much a topic under debate.

ACKNOWLEDGEMENTS

MS acknowledges support from the Royal Society. Research leading to these results has received funding from the European Research Council (ERC) under the European Union’s Seventh Framework Programme (FP7/2007–2013)/ERC Grant agreement no [291222] (PI: Smartt). AG is supported by the EU/FP7 via an ERC grant, and by Minerva/ARCHES and Kimmel awards. SH is supported by a Minerva/ARCHES award. GL is supported by the Swedish Research Council through grant No. 623-2011-7117.

Based on observations collected at the European Organisation for Astronomical Research in the Southern hemisphere, Chile, as part of PESSTO (the Public ESO Spectroscopic Survey for Transient Objects Survey) ESO programme ID 188.D-3003, as well as observations made with ESO Telescopes at the La Silla Paranal Observatory under programme ID 090.D-0828(A) and 089.D-0647(A). Based on observations (GS-2012B-Q-86) obtained at the Gemini Observatory, which is operated by the Association of Universities for Research in Astronomy, Inc., under a cooperative agreement with the NSF on behalf of the Gemini partnership: the National Science Foundation (United States), the National Research Council (Canada), CONICYT (Chile), the Australian Research Council (Australia), Ministério da Ciência, Tecnologia e Inovação (Brazil)

and Ministerio de Ciencia, Tecnología e Innovación Productiva (Argentina). Based in part on data from the 1.3 m telescope operated by the SMARTS consortium.

The Liverpool Telescope is operated on the island of La Palma by Liverpool John Moores University in the Spanish Observatorio del Roque de los Muchachos of the Instituto de Astrofísica de Canarias with financial support from the UK Science and Technology Facilities Council. Observations were obtained with the Samuel Oschin Telescope at the Palomar Observatory as part of the Palomar Transient factory project, a scientific collaboration between the California Institute of Technology, Columbia University, La Cumbres Observatory, the Lawrence Berkeley National Laboratory, the National Energy Research Scientific Computing Center, the University of Oxford and the Weizmann Institute of Science. The William Herschel Telescope is operated on the island of La Palma by the Isaac Newton Group in the Spanish Observatorio del Roque de los Muchachos of the Instituto de Astrofísica de Canarias. This paper uses observations obtained with facilities of the Las Cumbres Observatory Global Telescope. This research has made use of the NASA/IPAC Extragalactic Database (NED) which is operated by the Jet Propulsion Laboratory, California Institute of Technology, under contract with the National Aeronautics and Space Administration. Funding for the SDSS and SDSS-II has been provided by the Alfred P. Sloan Foundation, the Participating Institutions, the National Science Foundation, the U.S. Department of Energy, the National Aeronautics and Space Administration, the Japanese Monbukagakusho, the Max Planck Society and the Higher Education Funding Council for England. The SDSS Web Site is <http://www.sdss.org/>. The SDSS is managed by the Astrophysical Research Consortium for the Participating Institutions. The Participating Institutions are the American Museum of Natural History, Astrophysical Institute Potsdam, University of Basel, University of Cambridge, Case Western Reserve University, University of Chicago, Drexel University, Fermilab, the Institute for Advanced Study, the Japan Participation Group, Johns Hopkins University, the Joint Institute for Nuclear Astrophysics, the Kavli Institute for Particle Astrophysics and Cosmology, the Korean Scientist Group, the Chinese Academy of Sciences (LAMOST), Los Alamos National Laboratory, the Max-Planck-Institute for Astronomy (MPIA), the Max-Planck-Institute for Astrophysics (MPA), New Mexico State University, Ohio State University, University of Pittsburgh, University of Portsmouth, Princeton University, the United States Naval Observatory and the University of Washington.

REFERENCES

- Aldering G. et al., 2006, *ApJ*, 650, 510
 Amanullah R., Goobar A., 2011, *ApJ*, 735, 20
 Arsenijević V., Fabbro S., Mourão A. M., Rica da Silva A. J., 2008, *A&A*, 492, 535
 Badenes C., Borkowski K. J., Hughes J. P., Hwang U., Bravo E., 2006, *ApJ*, 645, 1373
 Baltay C. et al., 2012, *The Messenger*, 150, 34
 Bandiera R., 1987, *ApJ*, 319, 885
 Blondin S., Prieto J. L., Patat F., Challis P., Hicken M., Kirshner R. P., Matheson T., Modjaz M., 2009, *ApJ*, 693, 207
 Blondin S., Mandel K. S., Kirshner R. P., 2011, *A&A*, 526, A81
 Blondin S. et al., 2012, *AJ*, 143, 126
 Bloom J. S. et al., 2012, *ApJ*, 744, L17
 Brandt T. D., Tojeiro R., Aubourg É., Heavens A., Jimenez R., Strauss M. A., 2010, *AJ*, 140, 804
 Bronder T. J. et al., 2008, *A&A*, 477, 717
 Brown T. M. et al., 2013, preprint (arXiv:1305.2437)
 Burkey M. T., Reynolds S. P., Borkowski K. J., Blondin J. M., 2013, *ApJ*, 764, 63
 Childress M. et al., 2013a, *ApJ*, 770, 108
 Childress M. J., Filippenko A. V., Ganeshalingam M., Schmidt B. P., 2013b, preprint (arXiv:1307.0563)
 Chotard N. et al., 2011, *A&A*, 529, L4
 Conley A. et al., 2008, *ApJ*, 681, 482
 Cortés J. R., Kenney J. D. P., Hardy E., 2006, *AJ*, 131, 747
 Deng J. et al., 2004, *ApJ*, 605, L37
 Dennefeld M., 1982, *A&A*, 112, 215
 Di Stefano R., Voss R., Claeys J. S. W., 2011, *ApJ*, 738, L1
 Dilday B. et al., 2012, *Sci*, 337, 942
 Drake A. J. et al., 2009, *ApJ*, 696, 870
 Fisher A., Branch D., Hoflich P., Khokhlov A., 1995, *ApJ*, 447, L73
 Foley R. J., Sanders N. E., Kirshner R. P., 2011, *ApJ*, 742, 89
 Foley R. J. et al., 2012a, *ApJ*, 744, 38
 Foley R. J. et al., 2012b, *ApJ*, 752, 101
 Förster F., González-Gaitán S., Anderson J., Marchi S., Gutiérrez C., Hamuy M., Pignata G., Cartier R., 2012, *ApJ*, 754, L21
 Förster F., González-Gaitán S., Folatelli G., Morrell N., 2013, *ApJ*, 772, 19
 Gallagher J. S., Garnavich P. M., Berlind P., Challis P., Jha S., Kirshner R. P., 2005, *ApJ*, 634, 210
 Ganeshalingam M. et al., 2010, *ApJS*, 190, 418
 Gilfanov M., Bogdán Á., 2010, *Nat*, 463, 924
 Gomez H. L. et al., 2012, *MNRAS*, 420, 3557
 Goobar A., 2008, *ApJ*, 686, L103
 Guy J. et al., 2010, *A&A*, 523, A7
 Hamuy M., Phillips M. M., Maza J., Suntzeff N. B., Schommer R. A., Aviles R., 1995, *AJ*, 109, 1
 Hamuy M., Phillips M. M., Suntzeff N. B., Schommer R. A., Maza J., Aviles R., 1996, *AJ*, 112, 2391
 Hamuy M., Trager S. C., Pinto P. A., Phillips M. M., Schommer R. A., Ivanov V., Suntzeff N. B., 2000, *AJ*, 120, 1479
 Hamuy M. et al., 2003, *Nat*, 424, 651
 Hicken M. et al., 2009, *ApJ*, 700, 331
 Hicken M. et al., 2012, *ApJS*, 200, 12
 Howell D. A. et al., 2006, *Nat*, 443, 308
 Iben I., Tutukov A. V., 1984, *ApJS*, 54, 335
 Johansson J. et al., 2013, *MNRAS*, 435, 1680
 Justham S., 2011, *ApJ*, 730, L34
 Kato M., 2013, in Di Stefano R., Orio M., Moe M., eds, *Proc. IAU Symp.* 281, Binary Paths to Type Ia Supernovae Explosions. Cambridge Univ. Press, Cambridge, p. 145
 Kerzendorf W. E. et al., 2013, *ApJ*, 774, 99
 Kessler R. et al., 2009, *ApJS*, 185, 32
 Klotz A., Boër M., Eysseric J., Damerdjy Y., Laas-Bourez M., Pollas C., Vachier F., 2008, *PASP*, 120, 1298
 Kotak R., Meikle W. P. S., Adamson A., Leggett S. K., 2004, *MNRAS*, 354, L13
 Law N. M. et al., 2009, *PASP*, 121, 1395
 Leaman J., Li W., Chornock R., Filippenko A. V., 2011, *MNRAS*, 412, 1419
 Leloudas G. et al., 2013, preprint (arXiv:1306.1549)
 Leonard D. C., 2007, *ApJ*, 670, 1275
 Li W. et al., 2011, *Nat*, 480, 348
 Lundqvist P. et al., 2013, preprint (arXiv:1307.4099)
 Maguire K. et al., 2012, *MNRAS*, 426, 2359
 Mannucci F., della Valle M., Panagia N., Cappellaro E., Cresci G., Maiolino R., Petrosian A., Turatto M., 2005, *A&A*, 433, 807
 Mannucci F., Della Valle M., Panagia N., 2006, *MNRAS*, 370, 773
 Maoz D., Mannucci F., Brandt T. D., 2012, *MNRAS*, 426, 3282
 Marietta E., Burrows A., Fryxell B., 2000, *ApJS*, 128, 615
 Markwardt C. B., 2009, in Bohlender D. A., Durand D., Dowler P., eds, *ASP Conf. Ser. Vol. 411, Astronomical Data Analysis Software and Systems XVIII*. Astron. Soc. Pac., San Francisco, p. 251
 Mattila S., Lundqvist P., Sollerman J., Kozma C., Baron E., Fransson C., Leibundgut B., Nomoto K., 2005, *A&A*, 443, 649
 Mazzali P. A. et al., 2005, *ApJ*, 623, L37
 Mazzali P. A., Röpke F. K., Benetti S., Hillebrandt W., 2007, *Sci*, 315, 825

- Meng X.-C., Yang W.-M., 2011, *Res. Astron. Astrophys.*, 11, 965
- Meng X., Chen X., Han Z., 2007, *PASJ*, 59, 835
- Modigliani A. et al., 2010, in Silva D. R., Peck A. B., Soifer B. T., eds, *Proc. SPIE Conf. Ser. Vol. 7737, Observatory Operations: Strategies, Processes, and Systems III*. SPIE, Bellingham, p. 773728
- Mohamed S., Booth R., Podsiadlowski P., 2013, in Di Stefano R., Orio M., Moe M., eds, *Proc. IAU Symp. 281, Binary Paths to Type Ia Supernovae Explosions*. Cambridge Univ. Press, Cambridge, p. 195
- Munari U., Henden A., Belligoli R., Castellani F., Cherini G., Righetti G. L., Vagnozzi A., 2013, *New Astron.*, 20, 30
- Nugent P. E. et al., 2011, *Nat*, 480, 344
- Ofek E. O. et al., 2012, *PASP*, 124, 854
- Park S. et al., 2013, *ApJ*, 767, L10
- Patat F. et al., 2007, *Sci*, 317, 924
- Patat F., Chugai N. N., Podsiadlowski P., Mason E., Melo C., Pasquini L., 2011, *A&A*, 530, A63
- Patnaude D. J., Badenes C., Park S., Laming J. M., 2012, *ApJ*, 756, 6
- Perlmutter S. et al., 1999, *ApJ*, 517, 565
- Phillips M. M., 1993, *ApJ*, 413, L105
- Prieto J. L. et al., 2007, preprint (arXiv:0706.4088)
- Raskin C., Kasen D., 2013, *ApJ*, 772, 1
- Raskin C., Scannapieco E., Rhoads J., Della Valle M., 2009, *ApJ*, 707, 74
- Rau A. et al., 2009, *PASP*, 121, 1334
- Riess A. G. et al., 1998, *AJ*, 116, 1009
- Riess A. G. et al., 1999, *AJ*, 117, 707
- Riess A. G. et al., 2007, *ApJ*, 659, 98
- Ruiter A. J. et al., 2013, *MNRAS*, 429, 1425
- Scannapieco E., Bildsten L., 2005, *ApJ*, 629, L85
- Schaefer B. E., Pagnotta A., 2012, *Nat*, 481, 164
- Shappee B. J., Stanek K. Z., Pogge R. W., Garnavich P. M., 2013, *ApJ*, 762, L5
- Shen K. J., Guillochon J., Foley R. J., 2013, *ApJ*, 770, L35
- Silverman J. M., Kong J. J., Filippenko A. V., 2012a, *MNRAS*, 425, 1819
- Silverman J. M., Ganeshalingam M., Li W., Filippenko A. V., 2012b, *MNRAS*, 425, 1889
- Silverman J. M. et al., 2012c, *ApJ*, 756, L7
- Silverman J. M. et al., 2013, *ApJS*, 207, 3
- Simon J. D. et al., 2007, *ApJ*, 671, L25
- Simon J. D. et al., 2009, *ApJ*, 702, 1157
- Smith M. et al., 2012, *ApJ*, 755, 61
- Soker N., Kashi A., García-Berro E., Torres S., Camacho J., 2013, *MNRAS*, 431, 1541
- Steele I. A. et al., 2004, in Oschmann J. M., Jr, ed., *Proc. SPIE Conf. Ser. Vol. 5489, Ground-based Telescopes*. SPIE, Bellingham, p. 679
- Sternberg A. et al., 2011, *Sci*, 333, 856
- Stritzinger M. et al., 2010, *AJ*, 140, 2036
- Stritzinger M. D. et al., 2011, *AJ*, 142, 156
- Sullivan M. et al., 2006, *ApJ*, 648, 868
- Sullivan M. et al., 2010, *MNRAS*, 406, 782
- Sullivan M. et al., 2011, *ApJ*, 737, 102
- Suzuki N. et al., 2012, *ApJ*, 746, 85
- Taddia F. et al., 2012, *A&A*, 545, L7
- van Loon J. T. et al., 2013, *A&A*, 550, A108
- Vernet J. et al., 2011, *A&A*, 536, A105
- Walker E. S. et al., 2011, *MNRAS*, 410, 1262
- Wang L., Baade D., Höflich P., Wheeler J. C., Kawabata K., Nomoto K., 2004, *ApJ*, 604, L53
- Wang X. et al., 2008, *ApJ*, 675, 626
- Wang X. et al., 2009, *ApJ*, 699, L139
- Wang X., Wang L., Filippenko A. V., Zhang T., Zhao X., 2013, arXiv:e-prints
- Webbink R. F., 1984, *ApJ*, 277, 355
- Wells L. A. et al., 1994, *AJ*, 108, 2233
- Whelan J., Iben I. J., 1973, *ApJ*, 186, 1007
- Williams R., Mason E., Della Valle M., Ederoclite A., 2008, *ApJ*, 685, 451
- Wood-Vasey W. M., Wang L., Aldering G., 2004, *ApJ*, 616, 339
- Yaron O., Gal-Yam A., 2012, *PASP*, 124, 668
- Yoon S.-C., Podsiadlowski P., Rosswog S., 2007, *MNRAS*, 380, 933
- York D. G. et al., 2000, *AJ*, 120, 1579

APPENDIX A: S11 SAMPLE VALUES

Table A1. Information for S11 sample including light curve and spectral measurements. Si II 6355 Å velocities are measured SN line velocities in the phase range -2 to $+5$ d with respect to B -band maximum. The references for the photometric and spectral properties are given in Section 2.7.

SN	z_{helio}	Stretch	$B - V$ at max.	Na I D ₂ pEW (Å)	'Blueshifted' Na I D ₂ pEW (Å) ^h	Galaxy type	Si II 6355 Å vel. (10^3 km s^{-1})	Phase ⁱ (d)
Blueshifted Na I D								
SN 2006X	$0.005\,486 \pm 0.000\,006^a$	0.950 ± 0.010	1.22 ± 0.01	1.16 ± 0.03	0.46 ± 0.04	Sbc	15.68 ± 0.10	0
SN 2006cm*	$0.016\,434 \pm 0.000\,007^b$	1.007 ± 0.082	0.92 ± 0.02	1.10 ± 0.01	0.06 ± 0.02	Sb	11.01 ± 0.13	0
SN 2007af*	$0.005\,47^c$	0.967 ± 0.011	0.05 ± 0.01	0.20 ± 0.02	0.15 ± 0.03	Scd	10.42 ± 0.11	0
SN 2007le	$0.007\,13^d$	1.020 ± 0.016	0.33 ± 0.01	0.98 ± 0.02	0.98 ± 0.02	Sc	$12.83 \pm 0.13^*$	0 ^j
SN 2008C	$0.016\,925 \pm 0.000\,007^b$	0.777 ± 0.037	0.19 ± 0.02	0.64 ± 0.02	0.64 ± 0.02	S0/a	10.72 ± 0.15	+2
SN 2008ec	$0.016\,317 \pm 0.000\,007^e$	0.878 ± 0.011	0.15 ± 0.01	0.43 ± 0.01	0.43 ± 0.01	Sa	–	–
SN 2009ig	$0.008\,770 \pm 0.000\,021^e$	1.089 ± 0.048	0.06 ± 0.01	0.29 ± 0.02	0.29 ± 0.02	Sa	13.53 ± 0.13	0
SN 2009le*	$0.017\,458 \pm 0.000\,007^f$	1.076 ± 0.082	0.06 ± 0.07	1.16 ± 0.02	0.54 ± 0.03	Sbc	–	–
SN 2009ds*	$0.019\,032 \pm 0.000\,007^g$	1.089 ± 0.027	0.02 ± 0.02	0.66 ± 0.01	0.49 ± 0.03	Sc	–	–
SN 2010A*	$0.020\,698 \pm 0.000\,033^e$	1.015 ± 0.062	0.11 ± 0.02	0.47 ± 0.01	0.28 ± 0.03	Sab	–	–
Non-blueshifted Na I D								
SN 2007kk	$0.041\,045 \pm 0.000\,103^e$	1.098 ± 0.041	0.00 ± 0.02	0.47 ± 0.01	–	Sbc	–	–
SN 2008fp	$0.005\,664 \pm 0.000\,067^e$	1.067 ± 0.020	0.58 ± 0.02	1.20 ± 0.01	–	S0 pec	10.83 ± 0.10	0
No Na I D								
SN 2007on	$0.006\,494 \pm 0.000\,013^e$	0.702 ± 0.007	0.10 ± 0.01	–	–	E	11.06 ± 0.12	–1
SNF20080514-002	$0.022\,095 \pm 0.000\,090^e$	0.793 ± 0.024	-0.16 ± 0.02	–	–	S0	10.31 ± 0.16	+3
SN 2008hv	$0.012\,549 \pm 0.000\,067^e$	0.851 ± 0.011	0.01 ± 0.02	–	–	S0	10.90 ± 0.12	–1
SN 2008ia	$0.021\,942 \pm 0.000\,097^e$	0.880 ± 0.032	0.05 ± 0.03	–	–	E1	11.06 ± 0.18	+3

^aRedshift calculated from of CN lines in high-resolution UVES spectrum from Patat et al. (2007).^bRedshift from host galaxy features in SN spectrum.^cRedshift from H α emission from Simon et al. (2007).^dRedshift from H α emission from Simon et al. (2009).^eRedshift from recessional velocity obtained from NED or SDSS Data Release 9.^fRedshift from H α emission from high-resolution spectrum (Simon, private communication).^gRedshift from H α emission from high-resolution spectrum (Sternberg, private communication).^h'Blueshifted' Na I D pEW refers to the integrated pEW of any Na I D absorption features that are blueshifted with respect to the defined zero-velocity position.ⁱPhase with respect to B -band maximum, as measured using SiFTO^jAverage Si II 6355 Å velocity of -6 d and $+6$ d spectra.

*SN 2006cm, SN 2007af, SN 2009ds, SN 2009le and SN 2010A are removed from our calculation of the ratio of 'blueshifted' to 'redshifted' absorption features since they display both 'blueshifted' and 'non-blueshifted' Na I D absorption components.

This paper has been typeset from a \LaTeX file prepared by the author.